NASA Reference Publication 1214

1989

Limb-Darkening Functions as Derived From Along-Track Operation of the ERBE Scanning Radiometer for January 1985

G. Louis Smith
Langley Research Center
Hampton, Virginia

Natividad Manalo
PRC Kentron, Inc.
Aerospace Technologies Division
Hampton, Virginia

John T. Suttles
Langley Research Center
Hampton, Virginia

Ira J. Walker
PRC Kentron, Inc.
Aerospace Technologies Division
Hampton, Virginia

National Aeronautics and Space Administration
Office of Management
Scientific and Technical Information Division

Introduction

The interpretation of satellite measurements of longwave radiation, which is Earth-emitted radiation in the spectral range of 5 to 50 μm, requires the use of limb-darkening functions. The need for these functions was demonstrated by Lienesch and Wark (1967). Longwave radiance from a region decreases with increasing zenith angle of the ray due to the increasing path length through the cooler upper layers of the atmosphere. Limb-darkening functions describe this variation in longwave radiance with zenith angle and are necessary for relating radiance measurements to radiant exitances from the Earth-atmosphere system.

Raschke and Bandeen (1970) and Raschke et al. (1973) developed limb-darkening functions for various scene types by using available measurements and theoretical considerations for use in analyzing data from Medium Resolution Infrared Radiometers aboard the Nimbus 2 and 3 spacecraft. Taylor and Stowe (1984, 1986) developed anisotropy models for longwave and shortwave radiation from the Earth's atmosphere with data from the scanning radiometer of the Earth Radiation Budget (ERB) aboard the Nimbus 6 and 7 spacecraft (Smith et al. 1977; Jacobowitz et al. 1979). These models were extended by Suttles et al. (1989) for use in the analysis of scanning radiometer data from the Earth Radiation Budget Experiment (ERBE) (Smith et al. 1986). The ERBE scanning radiometer measures longwave radiances (5 to 50 μm) and shortwave radiances (0.2 to 5 μm) (Barkstrom and Smith 1986).

The scanning radiometer aboard the Earth Radiation Budget Satellite (ERBS) was rotated in azimuth to scan along track, that is, in the orbit plane, from approximately 1900 hours January 16, 1985, to 2100 hours January 28, 1985. This mode is depicted in figure 1, which shows that any site along the ground track of the spacecraft is viewed from a number of viewing zenith angles during a single orbital pass. Operation in this manner permits the study of a number of problems of measurement of the radiation field of the Earth. In particular, it provides data for developing a limb-darkening model for a single site over a short period of time rather than by compositing data taken at different times and different locations as is required by the use of most other data sets. Some limb-darkening models have been derived for desert scenes by Brooks (1986, 1987).

This paper presents a set of empirical limb-darkening models which were developed from the along-track data of January 17 through 27, 1985. The models are given both in graphical form and as tables. Models are developed separately for day and for night. The ERBS is in a 57° inclination orbit at an altitude of 600 km, which requires about 2 months to precess around the earth (Harrison et al. 1983). Because of the orbit, the data cover from 57°N to 57°S in latitude. Models are developed for a variety of scene types discriminated by surface type (ocean, land, snow, desert, and coastal) and cloudiness categories (clear, partly cloudy, mostly cloudy, and overcast), using the ERBE scene identification algorithm (Smith et al. 1986) with viewing zenith angles of less than 10°.

Method

The radiance L leaving the "top of the atmosphere" is related to the radiant exitance M by the limb-darkening function R:

$$L = \pi^{-1} R M \tag{1}$$

This relation permits one to compute the radiant exitance M from a measurement of radiance L in a single direction if the limb-darkening function R is known. The radiant exitance is given in terms of the radiance as

$$M = \int_{2\pi} d\Omega \, L \cos\theta \tag{2}$$

where Ω is the solid angle subtended at the radiating point and θ is the zenith angle of the exiting ray. From these two equations, it follows that R must satisfy the normalization condition

$$\pi^{-1} \int_{2\pi} d\Omega \, R \cos\theta = 1$$

As a consequence of this condition, $R > 1$ near zenith and $R < 1$ toward the limb.

In this paper, the usual assumption that the outgoing longwave radiation (OLR) is axisymmetric about the vertical is used. Brooks and Fenn (1988a) show cases in which topography can cause nonaxisymmetric effects on OLR, but such cases are quite localized and are not of significance for computations of radiant exitance from measurements that come from all locations over the Earth. With the assumption that the outgoing longwave radiance is axisymmetric, equation (2) simplifies to

$$M = 2\pi \int_0^{\pi/2} d\theta \, L \sin\theta \cos\theta \tag{3}$$

It is useful to define $z = \cos^2\theta$, so that equation (3) can be written as

$$M = \pi \int_0^1 dz \, L \tag{4}$$

For numerical evaluation with data, equation (4) is approximated by

$$M = \pi \sum_i \bar{L}_i \, \Delta z_i \tag{5}$$

where $\bar{L}_i$ is the average radiance in the ith angular bin and

$$\Delta z_i = \cos^2 \theta_i - \cos^2 \theta_{i+1}$$

This form has the advantage that no quadrature error is incurred for numerical integration for a Lambertian radiator.

In order to compute limb-darkening functions from along-track data, the radiant exitance M is computed from the measured radiances L by use of equation (5). The limb-darkening function $R(\theta)$ is then computed from equation (1), which gives

$$R(\theta) = \frac{\pi L(\theta)}{M} \tag{6}$$

For some cases, limb-darkening functions are expected to have differences between day and night. The primary case is for deserts, where the heating of the surface during the day and cooling at night causes the limb darkening to be greater during the day than during the night. For this reason, a set of limb-darkening models is developed for day and also for night.

Implementation of Method

As with most scanners, the ERBE pixel footprint on the Earth grows with viewing zenith angle. The pixel may be crudely approximated as a circular field of view with a diameter of 3.5° at the spacecraft, which gives a footprint of 37 km near nadir. As the scanner moves from nadir, the footprint width increases with the slant range, and the footprint length increases additionally as the secant of the zenith angle, as shown in figure 2. Because of the Earth's rotation, the center of these points at large viewing zenith angles is displaced from the ground track. This displacement of the pixel center from the sub-satellite track depends on the latitude and is also shown in figure 2. This displacement is small compared with the footprint and warrants no concern.

In order to implement this procedure by using equations (5) and (6), the orbit is partitioned into intervals 108 km long along the ground track, starting at the beginning of the data tape (Processed Archival Tape, or PAT) for the day. This length is convenient because every 16 sec the location of the spacecraft is recorded on the PAT. Also, it corresponds to the pixel length at 55° (fig. 2) so that it matches the pixel size in order of magnitude. The pixel centers are some finite distance from the ground track; therefore, the surface of the Earth is divided into strips by great circles normal to the orbit track at the interval ends. Each measurement is assigned to the interval within which the center of the pixel falls, as illustrated in figure 3, even though nearly half of the pixel may be in an adjacent interval. In the figure, the distance of the pixel center from the sub-satellite track is exaggerated. Also as indicated in the figure, the size and shape of the footprint of the pixel at the top of the atmosphere (taken to be a surface 30 km above the sea level) change with viewing zenith angle.

The average number of pixels in each interval is simply the number of measurements per orbit divided by the number of intervals covered per orbit. The scanning radiometer makes 62 measurements during each scan, and makes a scan every 4 sec. The spacecraft completes a 360° circuit of the Earth every 100 min. It follows that every interval has approximately 258 measurement pixels assigned to it.

For each interval, the scene types as computed by the ERBE scene identification algorithm (Smith et al. 1986) are compiled using each pixel which has a viewing zenith angle of less than 10°. The interval is specified to be of a scene type only if at least 80 percent of these pixels are computed to have that scene type. Intervals which are not specified to have a scene type by this criterion are not used any further. This procedure eliminates intervals with large scene type variations within them. For example, it permits up to 20 percent of the pixels to be classed as partly cloudy for the intervals used to develop clear sky models.

The fact that the scene can be identified near nadir is another advantage of the use of along-track data. This is because in a three-dimensional broken cloud field, the apparent cloudiness increases with viewing zenith angle, as shown in figure 4. For large viewing zenith angles only cloud tops are seen; therefore, it is difficult to distinguish broken cloud scenes from completely overcast scenes if only data from large viewing zenith angles are available.

The limb-darkening models are computed by use of equation (6) as follows. For each interval, the radiances are averaged in 18 viewing zenith angle bins of 5° each. Data for the two bins for 80° through 90° are not used due to time lag and field-of-view contamination by space. Values for these bins are obtained by linear extrapolation from the centers of the two adjacent bins. The error in the resulting radiant exitance is very small because Δz_i for these bins is quite small, and any error in L will have only a

small effect. The standard deviation of the radiances within each bin from 0° to 80° is computed, and if the standard deviation within any viewing zenith angle bin exceeds 1.5 percent of the mean radiance for that bin, the interval is rejected. If the interval is accepted, the radiant exitance for the interval is then computed by use of equation (5), and the limb-darkening function is computed by equation (6). The limb-darkening functions are averaged for all intervals for each scene type for each latitude band to produce the results reported here.

Because of the editing requirement that the standard deviation in any viewing zenith angle bin is less than 1.5 percent and the fact that there are many measurements in any one bin, the sampling error for any given interval is a fraction of a percent. Also, any error in gain of the radiometer will tend to cancel out in the calculation of the limb-darkening model through the use of equation (6), and any offset of the measurements is a fraction of a percent of the radiance. Thus, the limb-darkening model is accurate to a fraction of a percent for any one interval. The question then arises as to how representative is a given region for computation of the model. Because the variation between intervals is small for a given scene type and latitude range and based on examination of results, it is believed that 10 intervals provide sufficient sampling to define the limb-darkening model to a fraction of a percent.

Results

Limb-darkening functions have been generated for the ERBE scene identification classes for latitude zones as listed in table 1 for day and table 2 for night. The number in the table is the number of intervals which was used for the computation of the limb-darkening model. The latitude zones are those used for ERBE data inversion calculations and are strips 18° wide starting at the North Pole. Because the ERBS spacecraft is in an orbit with 57° inclination, it does not make observations poleward of 57°; thus, no data are taken in zones 1 and 10. The models for zones 2 and 9 are based on data only between 54° and 57° and are not representative of the full width of the zone. During the period of along-track scan, the ascending node of the spacecraft orbit precessed through less than 60° and was oriented such that the spacecraft was at the northern-most part of the orbit at night and likewise at the southern-most part of the orbit during the day. Thus, zone 2 was not observed during day and band 9 was not observed during night. Also, zones 3 and 4 had only a small number of observations during the day. There are other cases missing, many of which are irrelevant in the ERBE scene classification, such as desert in zone 9 or snow in zone 5.

Discrimination of cloud from snow is difficult with broadband radiometer data. Thus, the snow models may contain measurements made from overcast conditions. This is not expected to cause significant errors because the models are very similar. In both cases, the moisture above the radiating surface is usually low; thus, the limb darkening for each case is small.

The limb-darkening functions are shown in figures 5 through 14 for day and figures 15 through 26 for night. Also, they are presented in tables 3 and 4 for convenience of use in numerical application. For day, the limb-darkening functions have values of 1.04 to 1.09 at zenith, with 1.06 being typical. For night, the limb-darkening functions have values of 1.03 to 1.08 at zenith, with 1.06 being typical. It is found that latitude causes a variation on the order of 1 percent, except for zenith angles greater than 70°. For these large viewing zenith angles, there are stronger differences between the models. However, in the application of the models for zenith angles larger than 70°, scene identification errors are highly probable, such that the cloudiness of the scene is frequently overestimated. Thus, due to scene identification errors in this range in addition to bidirectional model errors, the data cannot be reliably analyzed for cross-track scanning. For this reason, ERBE data processing usually stops at viewing zenith angle of 70°.

Because of the similarity of the limb-darkening functions for the different cases, a mean function was formed for the day and one for the night, by averaging over all scene types and latitude zones, without weighting by population. These mean functions are listed in table 5 and shown in figure 27. At nadir and at 70°, the night and day functions differ by only 1 percent. They equal 1.0 at about 55°, as do most of the individual functions. Most scenes and latitudes differ by less than 2 percent from these mean functions. The desert differs from the average functions by less than 1 percent, contrary to expectations of large variations with viewing zenith angle and local time. The day models show a tendency at the 1-percent level to have more limb darkening in the Northern (winter) Hemisphere than in the Southern Hemisphere.

For the case of snow, it is difficult to discriminate between snow and cloud with broadband data. As a result, the snow model may include data from more cloud than other cases. Figure 17 shows snow to have about 2 percent more limb darkening at zenith than does overcast. Because snow is associated with cold air, hence with low absolute humidity, one does not expect a large degree of limb darkening for snow. It

is the opinion of the authors that the results given here for snow are not adversely affected by cloud contamination.

These data have the advantage that it is possible to categorize the scene from near zenith data and yet have measurements for large zenith angles. Also, for a given small region, a number of measurements are made from a number of zenith angles during a few minutes. Earlier models (e.g., Lienesch and Wark 1967, Suttles et al. 1989) were formed by the use of averages of data from different orbital passes, which tends to smooth the results. As a consequence, the present models are more limb darkened than were the earlier models.

Anomalously high radiances were found near the limb for partly cloudy over ocean and for mostly cloudy over ocean for the latitude zone between 36°S and 54°S. In these cases, the radiometer was looking toward the sunlit side of the ground track with solar zenith angles between 84° and 96°, at viewing zenith angles beyond 70°. This geometry corresponds to looking near the Sun, although the Sun was at least 15° outside the orbit plane, by along-track mission constraints. It is not clear whether the anomaly is due to sunlight being refracted by the atmosphere and misinterpreted as longwave radiation,[1] or is due to sunlight impinging on the radiometer more directly. Such anomalies have also been reported by Brooks and Fenn (1988b). In either case, these parameters are outside the limits of the usual data processing of ERBE data. For the present study, the limb-darkening functions were developed for these cases simply by using only the portion of the scan in which the radiometer was looking away from the Sun; thereby, the problem was obviated.

Concluding Remarks

Limb-darkening models have been developed by use of along-track scanning data from the scanning radiometer aboard the ERBS spacecraft during January 1985. These data have the advantage that it is possible to categorize the scene from near zenith data and yet to have measurements for large zenith angles. Also, for a given small region, a number of measurements are made from a number of zenith angles during a few minutes. Thus, it is not necessary to form averages which tend to smooth the results. Limb-darkening models are presented in tabular form and shown as figures for 10 scene types during the day and 12 scene types during the night for a range of latitude zones. The models are more limb darkened than earlier models. The limb-darkening models have values of 1.03 to 1.09 at zenith, with 1.06 being typical. It is found that latitude causes a variation on the order of 1 percent for viewing zenith angles less than 70°. Mean limb-darkening models for day and for night are computed; the individual limb-darkening models differ from these by less than 2 percent for most cases. The models presented here are about 2 percent more limb darkened than those derived from Nimbus 7 ERB data (NASA Reference Publication 1184, Vol. II). The reason for this small difference is as yet unknown.

[1] The longwave radiance for nighttime is computed primarily from the total channel because the total channel is more flat spectrally, and it is assumed that no shortwave component is present (Smith et al. 1986).

NASA Langley Research Center
Hampton, VA 23665-5225
January 18, 1989

References

Barkstrom, Bruce R.; and Smith, G. Louis 1986: The Earth Radiation Budget Experiment: Science and Implementation. *Reviews Geophys.*, vol. 24, no. 2, May, pp. 379–390.

Brooks, David R. 1986: Limb-Darkening Functions for the Earth-Atmosphere System Over Desert Scenes. *Sixth Conference on Atmospheric Radiation*, American Meteorological Soc., pp. J24–J27.

Brooks, David Robert 1987: Parameterized Angular Models for Interpreting Satellite-Based Measurements of Shortwave and Longwave Radiances Over Deserts. Ph.D. Thesis, Imperial College of Science and Technology, Univ. of London, Oct.

Brooks, David R.; and Fenn, Marta A. 1988a: *Summary of Along-Track Data From the Earth Radiation Budget Satellite for Several Major Desert Regions.* NASA RP-1197.

Brooks, David R.; and Fenn, Marta A. 1988b: *Summary of Along-Track Data From the Earth Radiation Budget Satellite for Several Representative Ocean Regions.* NASA RP-1206.

Harrison, Edwin F.; Minnis, Patrick; and Gibson, Gary G. 1983: Orbital and Cloud Cover Sampling Analyses for Multisatellite Earth Radiation Budget Experiments. *J. Spacecr. & Rockets*, vol. 20, no. 5, Sept./Oct., pp. 491–495.

Jacobowitz, H.; Smith, W. L.; Howell, H. B.; Nagle, F. W.; and Hickey, J. R. 1979: The First 18 Months of Planetary Radiation Budget Measurements From the Nimbus 6 ERB Experiment. *J. Atmos. Sci.*, vol. 36, no. 3, Mar., pp. 501–507.

Lienesch, J. H.; and Wark, D. Q. 1967: Infrared Limb Darkening of the Earth From Statistical Analysis of TIROS Data. *J. Appl. Meteorol.*, vol. 6, no. 4, Aug., pp. 674–682.

Raschke, E.; and Bandeen, W. R. 1970: The Radiation Balance of the Planet Earth From Radiation Measurements of the Satellite Nimbus II. *J. Appl. Meteorol.*, vol. 9, no. 2, Apr., pp. 215–238.

Raschke, Ehrhard: Vonder Haar, Thomas H.; Bandeen, William R.; and Pasternak, Musa 1973: The Annual Radiation Balance of the Earth-Atmosphere System During 1969-70 From Nimbus 3 Measurements. *J. Atmos. Sci.*, vol. 30, no. 3, Apr., pp. 341–364.

Smith, G. Louis; Green, Richard N.; Raschke, Ehrhard; Avis, Lee M.; Suttles, John T.; Wielicki, Bruce A.; and Davies, Roger 1986: Inversion Methods for Satellite Studies of the Earth's Radiation Budget: Development of Algorithms for the ERBE Mission. *Reviews Geophys.*, vol. 24, no. 2, May, pp. 407–421.

Smith, W. L.; Hickey, J.; Howell, H. B.; Jacobowitz, H.; Hilleary, D. T.; and Drummond, A. J. 1977: Nimbus-6 Earth Radiation Budget Experiment, *Appl. Opt.*, vol. 16, no. 2, Feb., pp. 306–318.

Suttles, J. T.; Green, R. N.; Smith, G. L.; Wielicki, B. A.; Walker, I. J.; Taylor, V. R.; and Stowe, L. L. 1989: *Angular Radiation Models for Earth-Atmosphere System. Volume II—Longwave Radiation.* NASA RP-1184, Vol. II.

Taylor, V. Ray; and Stowe, Larry L. 1984: Reflectance Characteristics of Uniform Earth and Cloud Surfaces Derived From NIMBUS 7 ERB. *J. Geophys. Res.*, vol. 89, no. D4, June 30, pp. 4987–4996.

Taylor, V. Ray; and Stowe, Larry L. 1986: Revised Reflectance and Emission Models From Nimbus-7 ERB Data. *Sixth Conference on Atmospheric Radiation*, American Meteorological Soc., pp. J19–J22.

Table 1. Number of Intervals Used to Develop Limb-Darkening Models for Day

Scene ID [a]	Number of intervals in latitude range, deg, of—							
	72N–54N (zone 2)	54N–36N (zone 3)	36N–18N (zone 4)	18N–0 (zone 5)	0–18S (zone 6)	18S–36S (zone 7)	36S–54S (zone 8)	54S–72S (zone 9)
Clear ocean	0	0	0	47	228	427	152	26
Clear land	0	0	3	25	0	29	0	0
Clear snow	0	0	0	0	0	0	0	0
Clear desert	0	0	2	0	0	0	0	0
Coast	0	0	0	0	2	3	3	0
PC/ocean	0	0	0	44	88	139	194	52
PC/land	0	0	0	19	4	33	5	0
PC/land-ocean	0	0	0	0	0	3	0	0
MC/ocean	0	0	2	4	6	51	644	367
MC/land	0	0	0	0	0	0	0	0
MC/land-ocean	0	0	0	0	0	0	3	0
Overcast	0	0	0	0	0	0	35	52

[a] MC, mostly cloudy; PC, partly cloudy.

Table 2. Number of Intervals Used to Develop Limb-Darkening Models for Night

Scene ID [a]	Number of intervals in latitude range, deg, of—							
	72N–54N (zone 2)	54N–36N (zone 3)	36N–18N (zone 4)	18N–0 (zone 5)	0–18S (zone 6)	18S–36S (zone 7)	36S–54S (zone 8)	54S–72S (zone 9)
Clear ocean	9	6	110	257	98	166	0	0
Clear land	0	0	6	87	0	2	0	0
Clear snow	252	375	0	0	0	0	0	0
Clear desert	0	0	70	32	0	18	0	0
Coast	0	0	2	2	0	0	0	0
PC/ocean	5	111	480	508	349	281	45	0
PC/land	0	27	244	65	12	55	2	0
PC/land-ocean	0	6	11	11	0	4	0	0
MC/ocean	181	261	91	14	15	14	25	0
MC/land	0	240	36	0	3	0	0	0
MC/land-ocean	14	9	0	0	0	0	0	0
Overcast	134	168	12	2	0	0	0	0

[a] MC, mostly cloudy; PC, partly cloudy.

Table 3. Limb-Darkening Models for Day

Scene ID [a]	Limb-darkening model for— Viewing zenith angle range, deg, of—																	
	0–5	5–10	10–15	15–20	20–25	25–30	30–35	35–40	40–45	45–50	50–55	55–60	60–65	65–70	70–75	75–80	80–85	85–90
Latitude: 36°N–18°N																		
Clear land	1.06	1.06	1.06	1.06	1.06	1.05	1.04	1.04	1.03	1.02	1.01	0.99	0.97	0.94	0.90	0.83	0.76	0.70
Clear desert	1.07	1.07	1.07	1.07	1.06	1.06	1.05	1.04	1.03	1.02	1.00	0.99	0.96	0.93	0.88	0.82	0.75	0.69
MC/ocean	1.05	1.06	1.05	1.05	1.05	1.05	1.04	1.04	1.03	1.02	1.01	0.99	0.98	0.95	0.90	0.83	0.76	0.68
Latitude: 18°N–0°																		
Clear ocean	1.07	1.07	1.07	1.07	1.06	1.06	1.05	1.04	1.03	1.02	1.01	0.99	0.97	0.93	0.88	0.80	0.73	0.65
Clear land	1.08	1.08	1.08	1.08	1.07	1.07	1.06	1.05	1.04	1.02	1.01	0.98	0.96	0.92	0.87	0.79	0.71	0.64
PC/ocean	1.08	1.08	1.08	1.07	1.07	1.06	1.06	1.05	1.04	1.02	1.01	0.98	0.96	0.92	0.87	0.79	0.71	0.63
PC/land	1.08	1.08	1.07	1.07	1.07	1.06	1.05	1.05	1.04	1.02	1.01	0.98	0.96	0.93	0.88	0.81	0.73	0.66
MC/ocean	1.06	1.06	1.06	1.05	1.05	1.05	1.04	1.04	1.03	1.02	1.01	0.99	0.97	0.95	0.90	0.84	0.77	0.70
Latitude: 0°–18°S																		
Clear ocean	1.07	1.07	1.06	1.06	1.06	1.06	1.05	1.04	1.03	1.02	1.01	0.99	0.97	0.94	0.89	0.81	0.74	0.66
Coast	1.07	1.06	1.06	1.06	1.06	1.06	1.05	1.04	1.03	1.02	1.01	0.99	0.97	0.94	0.88	0.81	0.74	0.66
PC/ocean	1.08	1.08	1.08	1.07	1.07	1.07	1.06	1.05	1.04	1.03	1.01	0.98	0.96	0.92	0.87	0.79	0.71	0.63
PC/land	1.09	1.08	1.08	1.08	1.08	1.07	1.06	1.05	1.04	1.02	1.01	0.98	0.95	0.92	0.87	0.78	0.70	0.61
MC/ocean	1.07	1.07	1.06	1.06	1.06	1.06	1.05	1.04	1.03	1.02	1.00	0.98	0.96	0.94	0.89	0.82	0.75	0.68
Latitude: 18°S–36°S																		
Clear ocean	1.07	1.06	1.06	1.06	1.06	1.06	1.05	1.04	1.03	1.02	1.01	0.99	0.97	0.94	0.89	0.81	0.74	0.66
Clear land	1.09	1.09	1.09	1.08	1.08	1.07	1.06	1.05	1.04	1.03	1.01	0.98	0.96	0.92	0.86	0.77	0.68	0.58
Coast	1.05	1.05	1.05	1.05	1.05	1.05	1.04	1.04	1.03	1.02	1.01	0.99	0.98	0.95	0.91	0.84	0.76	0.69
PC/ocean	1.07	1.07	1.06	1.06	1.06	1.06	1.05	1.04	1.03	1.02	1.01	0.99	0.97	0.94	0.89	0.81	0.74	0.66
PC/land	1.08	1.08	1.07	1.07	1.07	1.06	1.06	1.05	1.04	1.02	1.01	0.99	0.96	0.93	0.87	0.80	0.72	0.64
PC/land-ocean	1.06	1.06	1.06	1.06	1.06	1.05	1.05	1.04	1.03	1.02	1.00	0.99	0.97	0.94	0.90	0.83	0.76	0.69
MC/ocean	1.06	1.05	1.05	1.05	1.05	1.05	1.04	1.04	1.03	1.02	1.01	0.99	0.98	0.95	0.91	0.83	0.75	0.68
Latitude: 36°S–54°S																		
Clear ocean	1.06	1.06	1.06	1.06	1.06	1.06	1.05	1.04	1.03	1.02	1.01	0.99	0.97	0.94	0.89	0.80	0.71	0.62
Coast	1.06	1.06	1.06	1.06	1.06	1.05	1.05	1.04	1.03	1.03	1.01	0.99	0.97	0.95	0.90	0.80	0.70	0.60
PC/ocean	1.06	1.06	1.06	1.06	1.06	1.05	1.05	1.04	1.03	1.02	1.01	0.99	0.97	0.94	0.90	0.81	0.73	0.65
PC/land	1.08	1.08	1.07	1.07	1.07	1.06	1.06	1.05	1.04	1.03	1.01	0.99	0.96	0.92	0.87	0.78	0.69	0.60
MC/ocean	1.06	1.05	1.05	1.05	1.05	1.05	1.04	1.04	1.03	1.02	1.01	1.00	0.98	0.95	0.91	0.82	0.74	0.66
MC/land-ocean	1.06	1.06	1.05	1.05	1.05	1.05	1.04	1.04	1.03	1.02	1.01	1.00	0.98	0.95	0.90	0.82	0.73	0.65
Overcast	1.05	1.05	1.05	1.05	1.05	1.04	1.04	1.03	1.03	1.02	1.01	1.00	0.98	0.96	0.92	0.84	0.76	0.68
Latitude: 54°S–72°S																		
Clear ocean	1.06	1.06	1.06	1.06	1.06	1.05	1.05	1.04	1.03	1.02	1.01	0.99	0.98	0.95	0.90	0.81	0.71	0.62
PC/ocean	1.06	1.06	1.06	1.06	1.05	1.05	1.05	1.04	1.03	1.02	1.01	0.99	0.98	0.95	0.90	0.81	0.73	0.64
MC/ocean	1.05	1.05	1.05	1.05	1.05	1.05	1.04	1.04	1.03	1.02	1.01	1.00	0.98	0.96	0.91	0.82	0.74	0.65
Overcast	1.04	1.04	1.04	1.04	1.04	1.04	1.03	1.03	1.02	1.02	1.01	1.00	0.99	0.97	0.93	0.85	0.77	0.69

[a] MC, mostly cloudy; PC, partly cloudy.

Table 4. Limb-Darkening Models for Night

Scene ID [a]	Limb-darkening model for— Viewing zenith angle range, deg, of—																	
	0–5	5–10	10–15	15–20	20–25	25–30	30–35	35–40	40–45	45–50	50–55	55–60	60–65	65–70	70–75	75–80	80–85	85–90
Latitude: 72°N–54°N																		
Clear ocean	1.07	1.06	1.06	1.06	1.06	1.05	1.05	1.04	1.03	1.02	1.01	0.99	0.97	0.93	0.89	0.82	0.76	0.69
Clear snow	1.05	1.05	1.05	1.05	1.04	1.04	1.04	1.03	1.03	1.02	1.01	0.99	0.98	0.95	0.92	0.86	0.80	0.74
PC/ocean	1.07	1.07	1.06	1.06	1.06	1.06	1.05	1.04	1.03	1.02	1.01	0.99	0.97	0.93	0.88	0.81	0.74	0.67
MC/ocean	1.06	1.06	1.06	1.06	1.05	1.05	1.05	1.04	1.03	1.02	1.01	0.99	0.97	0.94	0.90	0.83	0.77	0.71
MC/land-ocean	1.06	1.05	1.05	1.05	1.05	1.05	1.04	1.04	1.03	1.02	1.01	0.99	0.97	0.95	0.90	0.84	0.78	0.72
Overcast	1.03	1.03	1.03	1.03	1.03	1.03	1.03	1.02	1.02	1.02	1.01	1.00	0.99	0.97	0.94	0.89	0.84	0.78
Latitude: 54°N–36°N																		
Clear ocean	1.07	1.07	1.07	1.07	1.06	1.06	1.05	1.04	1.04	1.02	1.01	0.99	0.96	0.93	0.88	0.80	0.72	0.63
Clear snow	1.04	1.04	1.04	1.04	1.04	1.04	1.03	1.03	1.02	1.02	1.01	1.00	0.98	0.96	0.92	0.86	0.81	0.75
PC/ocean	1.07	1.06	1.06	1.06	1.06	1.05	1.05	1.04	1.03	1.02	1.01	0.99	0.97	0.94	0.89	0.81	0.74	0.66
PC/land	1.05	1.05	1.05	1.05	1.05	1.04	1.04	1.03	1.03	1.02	1.01	0.99	0.98	0.95	0.91	0.84	0.78	0.71
PC/land-ocean	1.07	1.07	1.06	1.06	1.06	1.06	1.05	1.04	1.03	1.02	1.01	0.99	0.97	0.94	0.88	0.80	0.73	0.65
MC/ocean	1.06	1.06	1.06	1.06	1.05	1.05	1.05	1.04	1.03	1.02	1.01	0.99	0.97	0.94	0.90	0.83	0.77	0.70
MC/land	1.04	1.04	1.04	1.04	1.04	1.04	1.03	1.03	1.02	1.02	1.01	1.00	0.98	0.96	0.92	0.87	0.81	0.75
MC/land-ocean	1.06	1.06	1.06	1.06	1.06	1.05	1.05	1.04	1.03	1.02	1.01	0.99	0.97	0.94	0.89	0.83	0.76	0.70
Overcast	1.03	1.03	1.03	1.03	1.03	1.03	1.02	1.02	1.02	1.01	1.01	1.00	0.99	0.97	0.95	0.90	0.85	0.80
Latitude: 36°N–18°N																		
Clear ocean	1.06	1.06	1.06	1.06	1.06	1.05	1.05	1.04	1.03	1.02	1.01	0.99	0.97	0.94	0.89	0.82	0.75	0.69
Clear land	1.06	1.06	1.05	1.05	1.05	1.05	1.04	1.03	1.03	1.02	1.01	0.99	0.97	0.95	0.91	0.85	0.79	0.74
Clear desert	1.05	1.05	1.05	1.05	1.05	1.04	1.04	1.03	1.03	1.02	1.01	0.99	0.98	0.95	0.91	0.86	0.80	0.74
Coast	1.06	1.06	1.06	1.06	1.05	1.05	1.05	1.04	1.03	1.02	1.01	0.99	0.97	0.94	0.90	0.83	0.77	0.70
PC/ocean	1.06	1.06	1.06	1.06	1.06	1.05	1.05	1.04	1.03	1.02	1.01	0.99	0.97	0.94	0.89	0.83	0.76	0.69
PC/land	1.05	1.05	1.05	1.05	1.04	1.04	1.04	1.03	1.03	1.02	1.01	0.99	0.98	0.95	0.92	0.86	0.80	0.74
PC/land-ocean	1.06	1.06	1.06	1.06	1.06	1.05	1.05	1.04	1.03	1.02	1.01	0.99	0.97	0.94	0.89	0.83	0.76	0.69
MC/ocean	1.05	1.05	1.05	1.05	1.05	1.04	1.04	1.03	1.03	1.02	1.01	0.99	0.97	0.95	0.91	0.85	0.79	0.73
MC/land	1.04	1.04	1.04	1.04	1.04	1.04	1.03	1.03	1.02	1.02	1.01	1.00	0.98	0.96	0.93	0.87	0.81	0.75
Overcast	1.04	1.03	1.03	1.03	1.03	1.03	1.03	1.02	1.02	1.01	1.01	1.00	0.99	0.97	0.94	0.89	0.84	0.79
Latitude: 18°N–0°																		
Clear ocean	1.06	1.06	1.06	1.06	1.06	1.05	1.05	1.04	1.03	1.02	1.01	0.99	0.97	0.94	0.89	0.82	0.75	0.69
Clear land	1.06	1.06	1.06	1.06	1.06	1.05	1.05	1.04	1.03	1.02	1.01	0.99	0.97	0.94	0.89	0.82	0.76	0.69
Clear desert	1.05	1.05	1.05	1.05	1.05	1.04	1.04	1.03	1.03	1.02	1.01	0.99	0.97	0.95	0.91	0.85	0.79	0.74
Coast	1.06	1.06	1.06	1.06	1.05	1.05	1.05	1.04	1.03	1.02	1.01	0.99	0.97	0.94	0.89	0.83	0.77	0.71
PC/ocean	1.07	1.07	1.06	1.06	1.06	1.05	1.05	1.04	1.03	1.02	1.01	0.99	0.97	0.94	0.89	0.82	0.75	0.68
PC/land	1.06	1.06	1.06	1.06	1.06	1.05	1.05	1.04	1.03	1.02	1.01	0.99	0.97	0.94	0.89	0.82	0.75	0.68
PC/land-ocean	1.06	1.06	1.06	1.06	1.06	1.05	1.05	1.04	1.03	1.02	1.01	0.99	0.97	0.94	0.89	0.83	0.77	0.70
MC/ocean	1.06	1.06	1.06	1.06	1.06	1.05	1.05	1.04	1.03	1.02	1.01	0.99	0.97	0.94	0.89	0.82	0.75	0.69
Overcast	1.06	1.06	1.06	1.06	1.06	1.05	1.05	1.04	1.04	1.03	1.01	0.99	0.97	0.94	0.89	0.81	0.73	0.65
Latitude: 0°–18°S																		
Clear ocean	1.06	1.06	1.06	1.06	1.06	1.05	1.05	1.04	1.03	1.02	1.01	0.99	0.97	0.94	0.89	0.83	0.76	0.69
PC/ocean	1.07	1.07	1.07	1.07	1.06	1.06	1.05	1.04	1.03	1.02	1.01	0.99	0.97	0.93	0.88	0.81	0.74	0.67
PC/land	1.07	1.07	1.07	1.07	1.06	1.06	1.05	1.04	1.03	1.02	1.01	0.99	0.97	0.93	0.88	0.81	0.73	0.66
MC/ocean	1.06	1.06	1.06	1.06	1.05	1.05	1.04	1.04	1.03	1.02	1.01	0.99	0.97	0.94	0.90	0.83	0.77	0.70
MC/land	1.08	1.08	1.08	1.08	1.08	1.07	1.06	1.05	1.04	1.03	1.02	0.99	0.97	0.91	0.84	0.75	0.66	0.57
Latitude: 18°S–36°S																		
Clear ocean	1.06	1.06	1.06	1.06	1.05	1.05	1.04	1.04	1.03	1.02	1.01	0.99	0.97	0.94	0.90	0.84	0.78	0.72
Clear land	1.08	1.08	1.08	1.07	1.07	1.06	1.05	1.05	1.04	1.03	1.01	0.99	0.96	0.92	0.87	0.79	0.72	0.65
Clear desert	1.05	1.05	1.05	1.05	1.05	1.04	1.04	1.03	1.03	1.02	1.01	0.99	0.98	0.95	0.91	0.86	0.80	0.75
PC/ocean	1.06	1.06	1.06	1.05	1.05	1.05	1.04	1.03	1.03	1.02	1.01	0.99	0.97	0.94	0.90	0.84	0.79	0.73
PC/land	1.06	1.06	1.06	1.05	1.05	1.05	1.04	1.03	1.03	1.02	1.01	0.99	0.97	0.95	0.91	0.84	0.78	0.72
PC/land-ocean	1.06	1.05	1.05	1.05	1.05	1.04	1.04	1.03	1.02	1.02	1.01	0.99	0.98	0.95	0.92	0.85	0.79	0.73
MC/ocean	1.05	1.05	1.05	1.05	1.05	1.04	1.04	1.03	1.03	1.02	1.01	0.99	0.98	0.95	0.91	0.86	0.80	0.75
Latitude: 36°S–54°S																		
PC/ocean	1.05	1.05	1.05	1.05	1.04	1.04	1.04	1.03	1.02	1.01	1.00	0.99	0.97	0.95	0.92	0.87	0.82	0.77
PC/land	1.06	1.06	1.06	1.06	1.05	1.05	1.05	1.04	1.03	1.02	1.00	0.99	0.97	0.94	0.90	0.83	0.77	0.70
MC/ocean	1.04	1.04	1.04	1.04	1.04	1.04	1.03	1.03	1.02	1.01	1.00	0.99	0.98	0.96	0.93	0.88	0.82	0.76

[a] MC, mostly cloudy; PC, partly cloudy.

Table 5. Mean Limb-Darkening Models for Day and Night

Viewing zenith angle range, deg	Average limb-darkening model	
	Day	Night
0–5	1.066	1.057
5–10	1.065	1.056
10–15	1.062	1.056
15–20	1.061	1.055
20–25	1.060	1.052
25–30	1.056	1.048
30–35	1.049	1.044
35–40	1.042	1.036
40–45	1.032	1.029
45–50	1.021	1.020
50–55	1.009	1.010
55–60	0.989	0.991
60–65	0.970	0.973
65–70	0.940	0.944
70–75	0.892	0.901
75–80	0.812	0.837
80–85	0.733	0.773
85–90	0.653	0.709

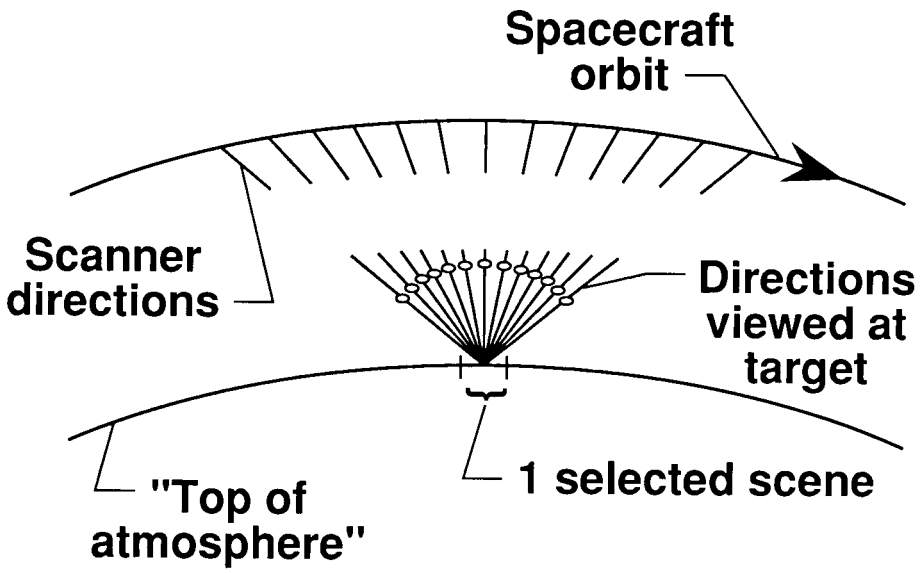

Figure 1. Use of along-track scanning for determining limb-darkening functions.

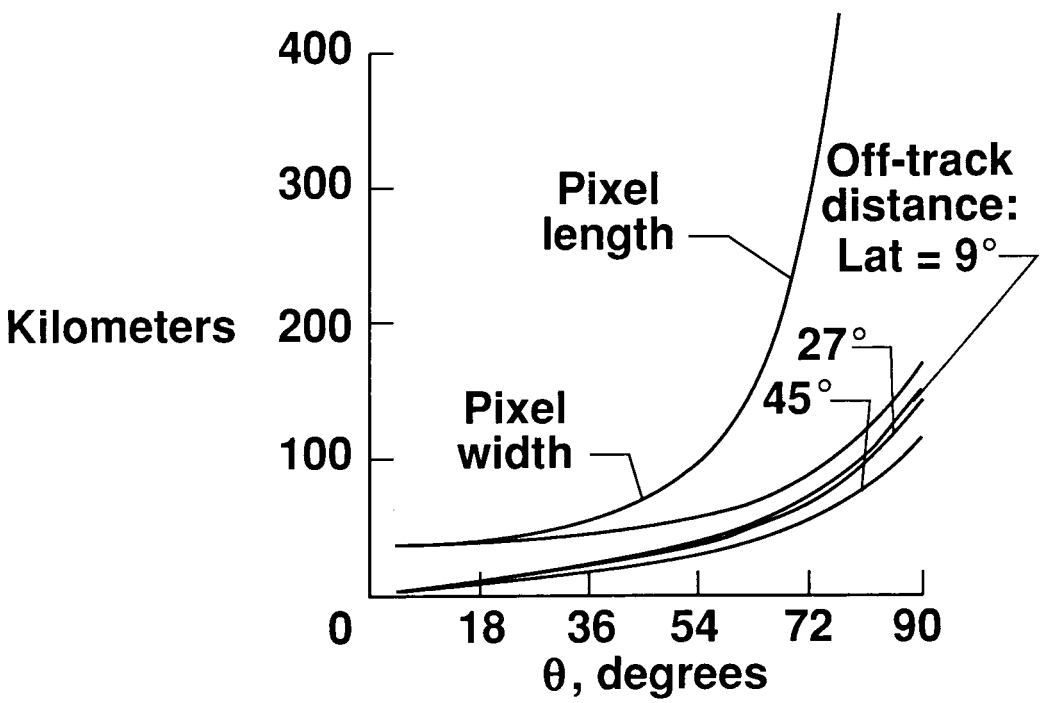

Figure 2. Growth of pixel footprint and displacement by Earth's rotation with zenith angle.

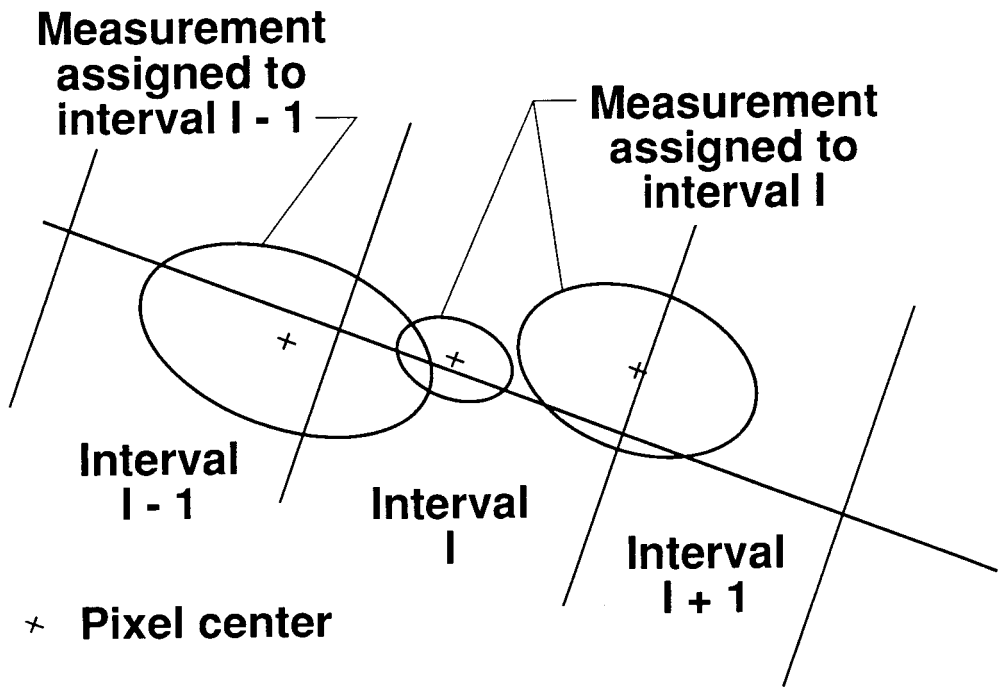

Figure 3. Allocation of measurements to intervals.

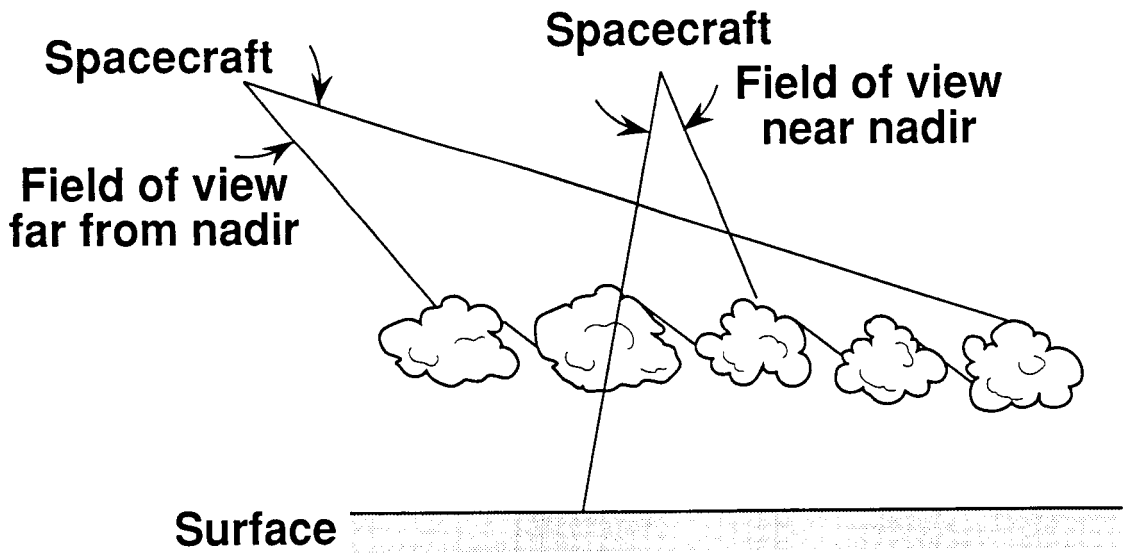

Figure 4. Effect of viewing zenith angle on apparent cloudiness.

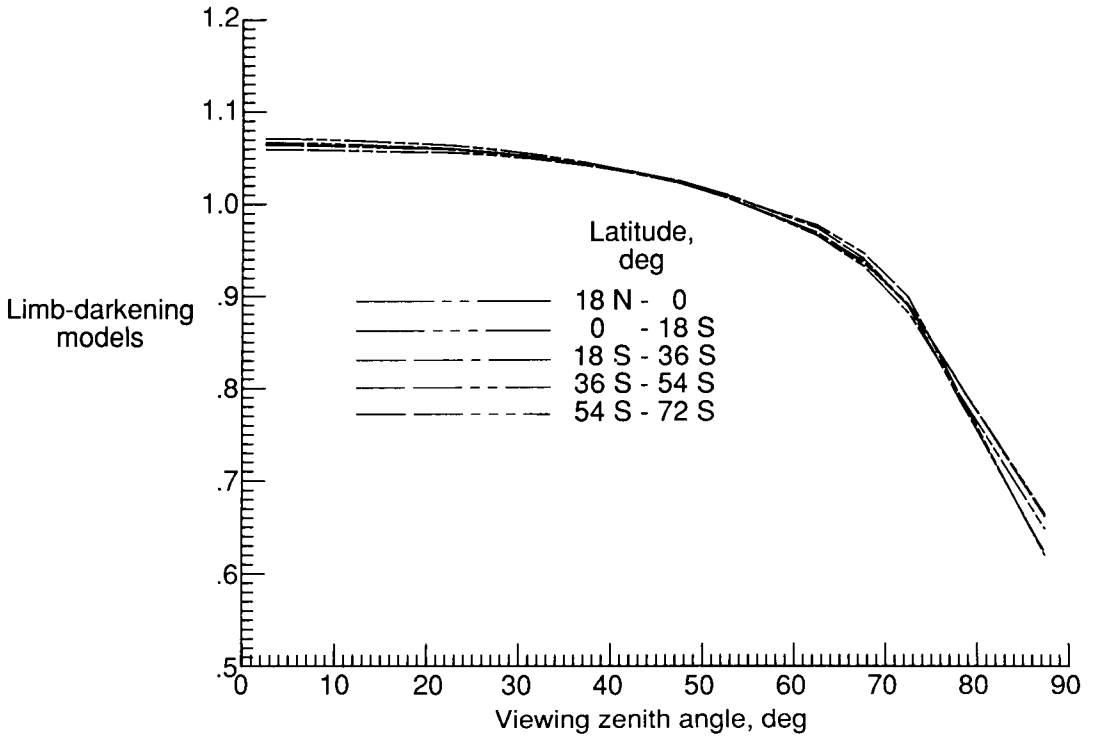

Figure 5. Limb-darkening models for clear ocean for day.

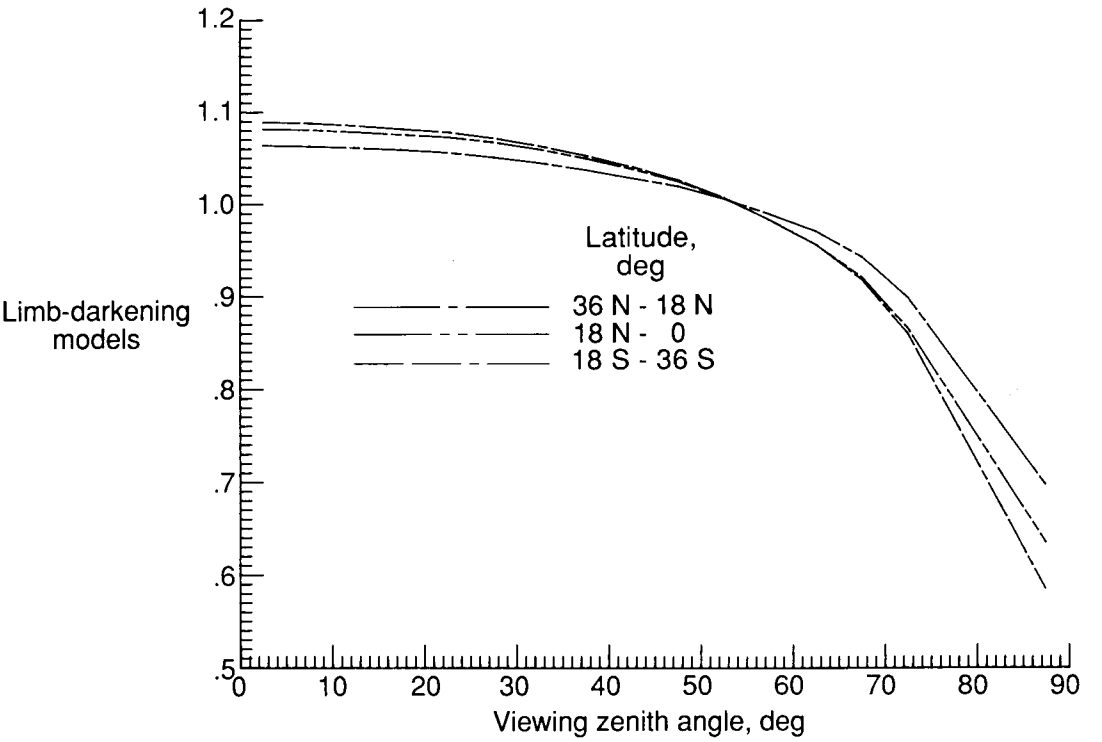

Figure 6. Limb-darkening models for clear land for day.

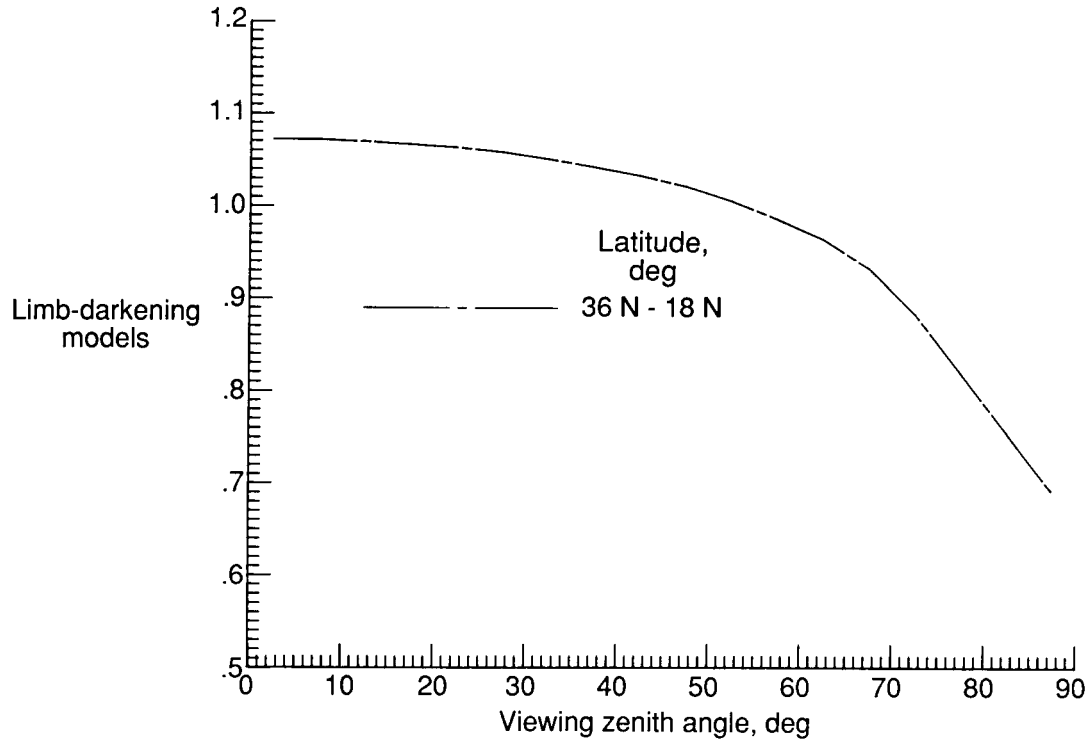

Figure 7. Limb-darkening models for clear desert for day.

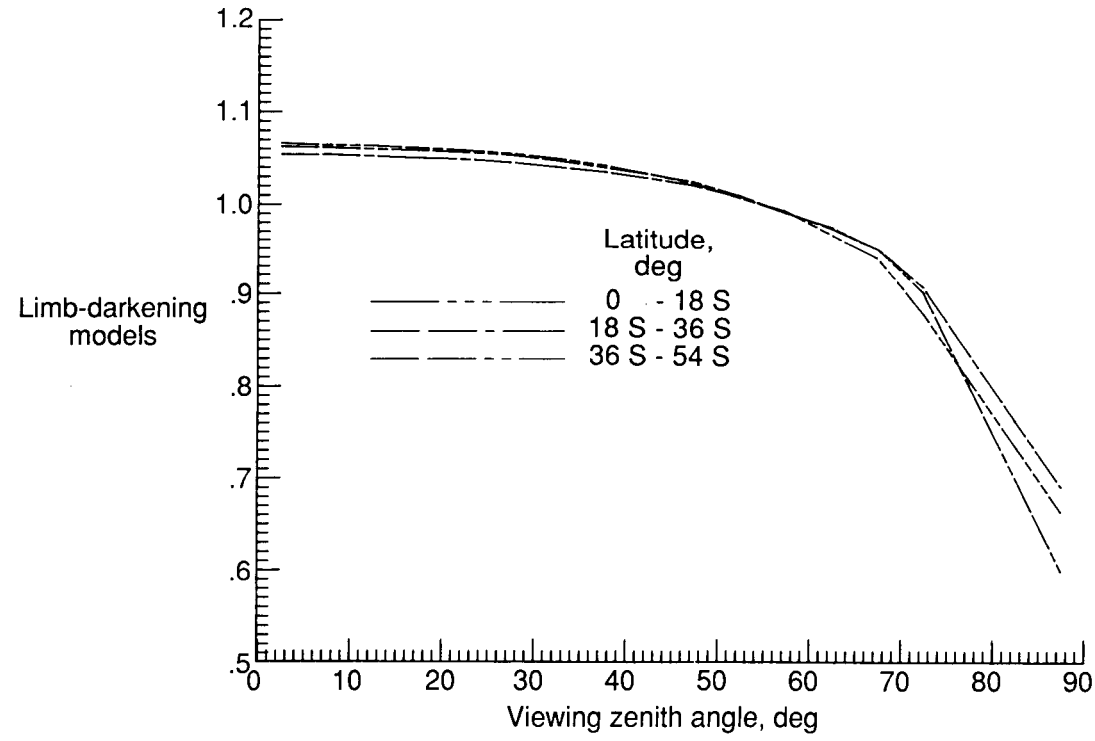

Figure 8. Limb-darkening models for clear land-ocean mix for day.

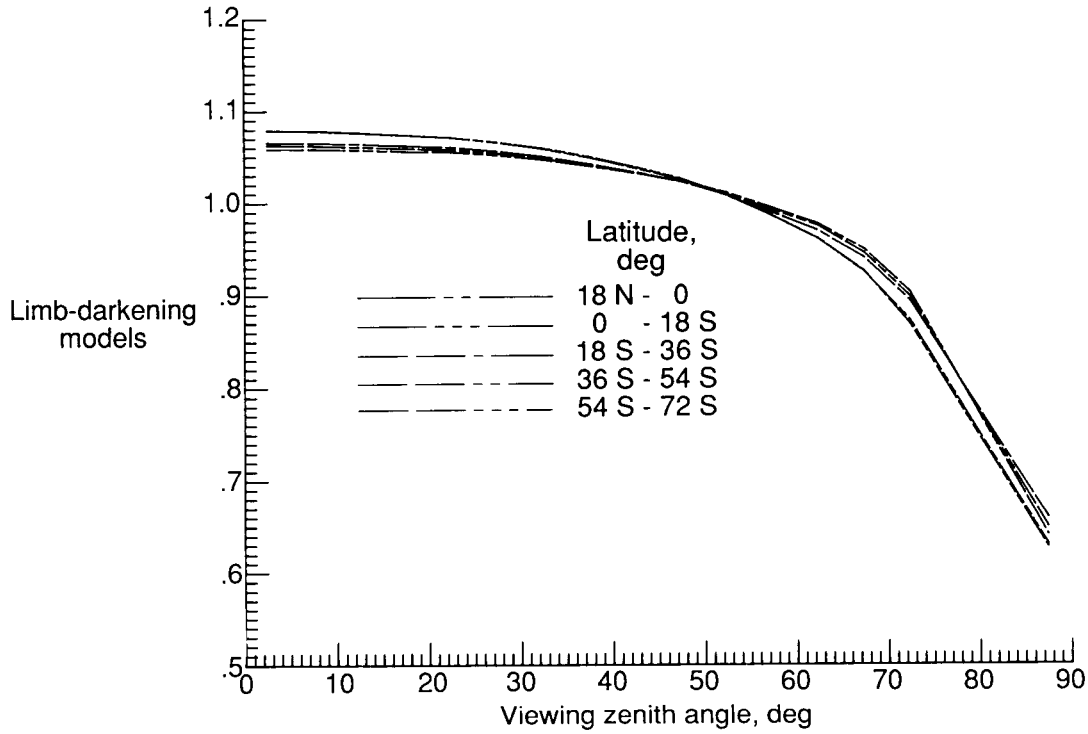

Figure 9. Limb-darkening models for partly cloudy over ocean for day.

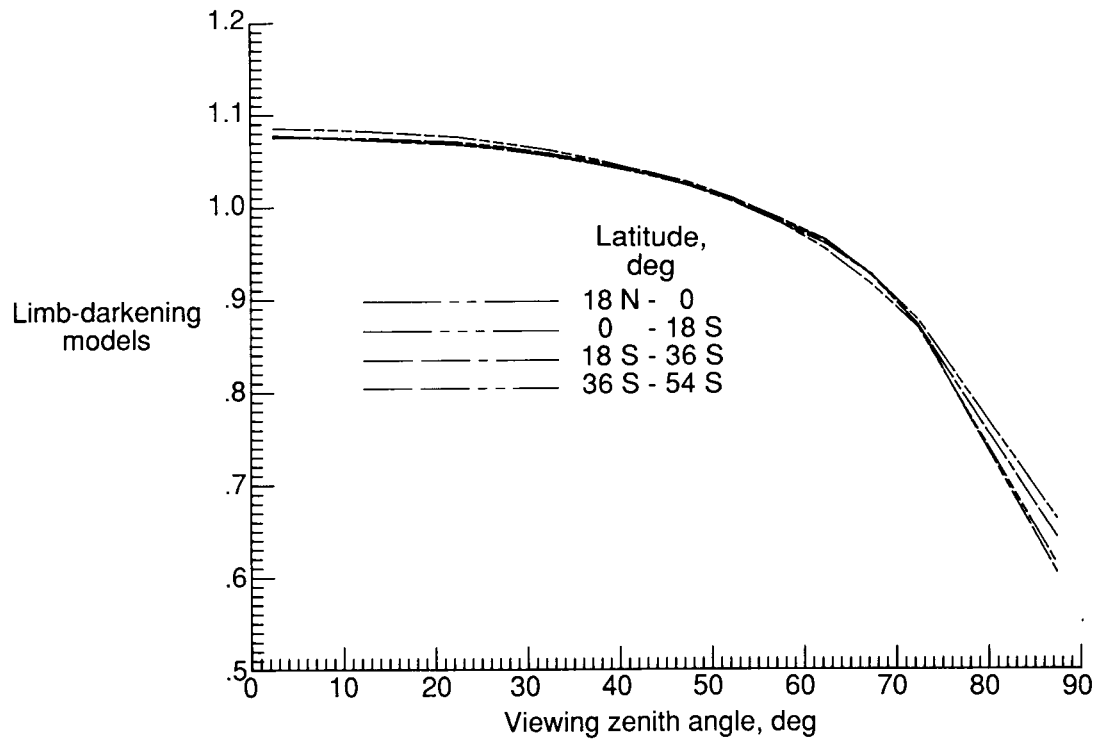

Figure 10. Limb-darkening models for partly cloudy over land for day.

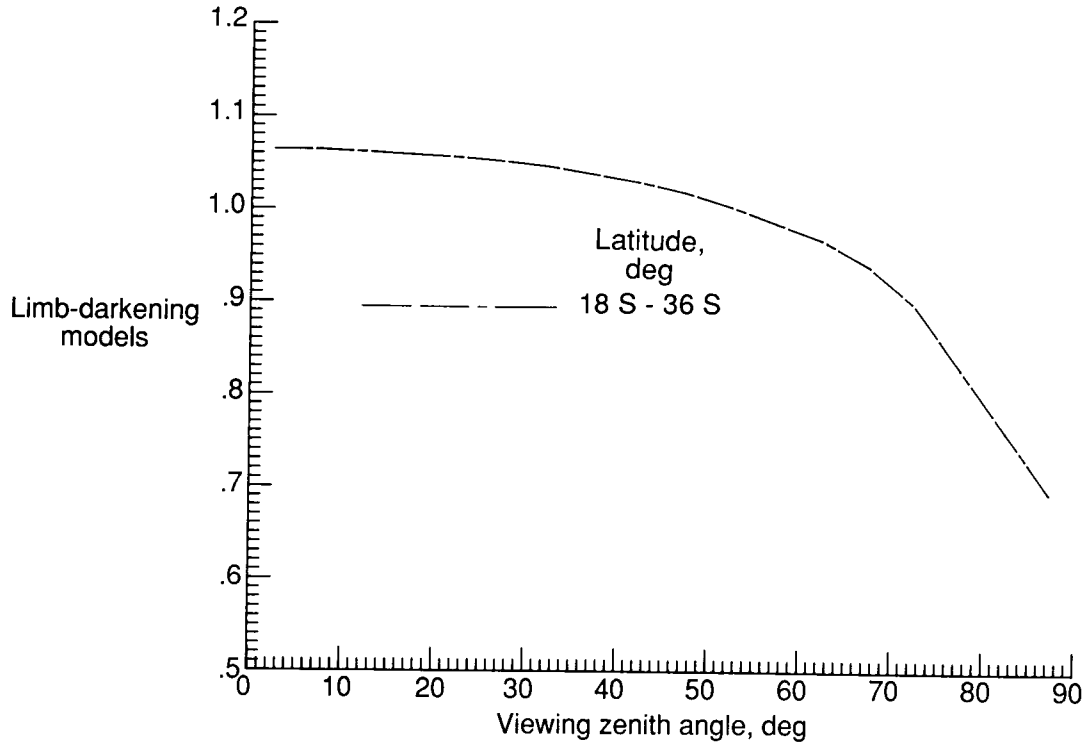

Figure 11. Limb-darkening models for partly cloudy over land-ocean mix for day.

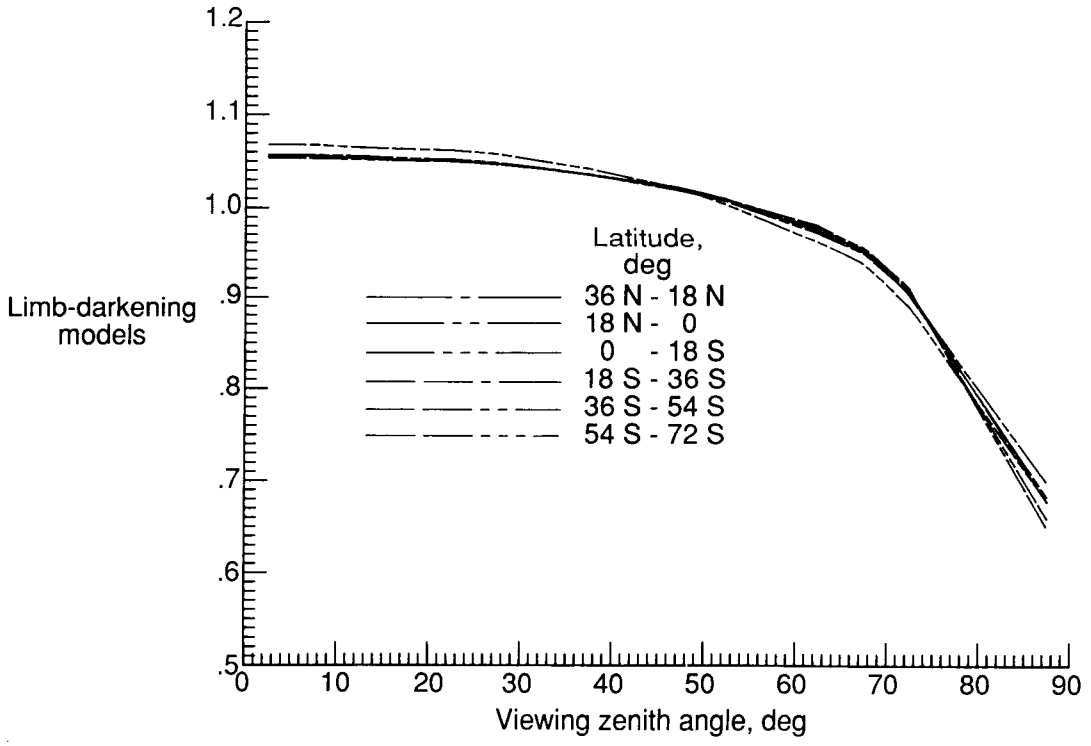

Figure 12. Limb-darkening models for mostly cloudy over ocean for day.

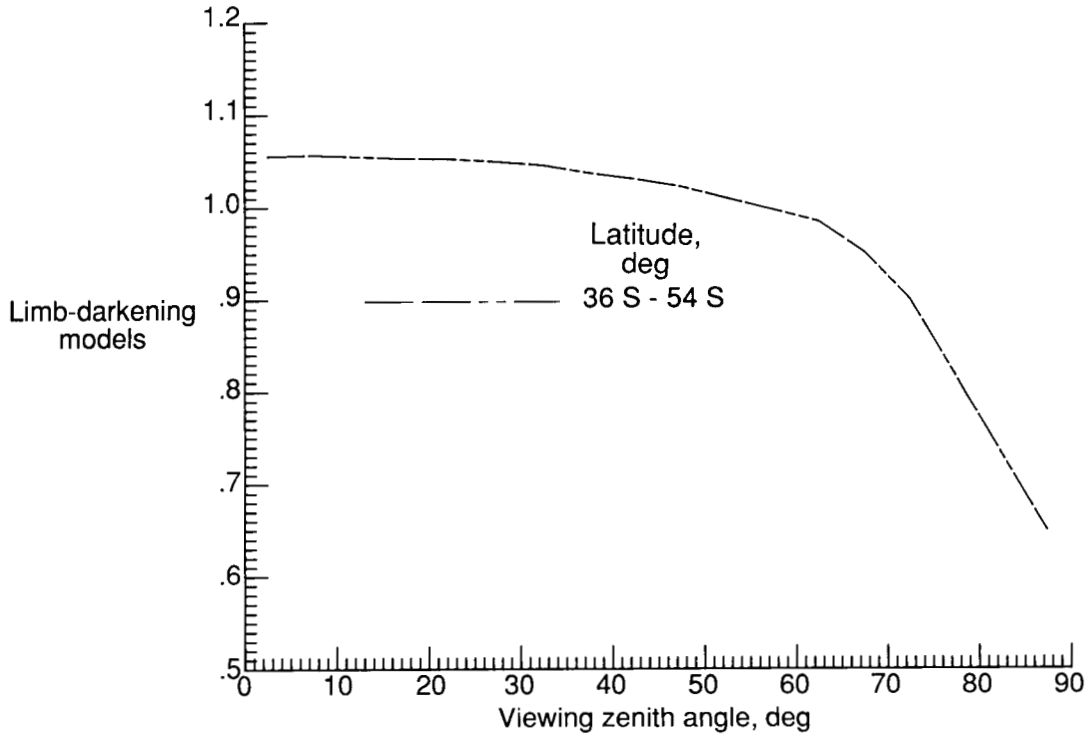

Figure 13. Limb-darkening models for mostly cloudy over land-ocean mix for day.

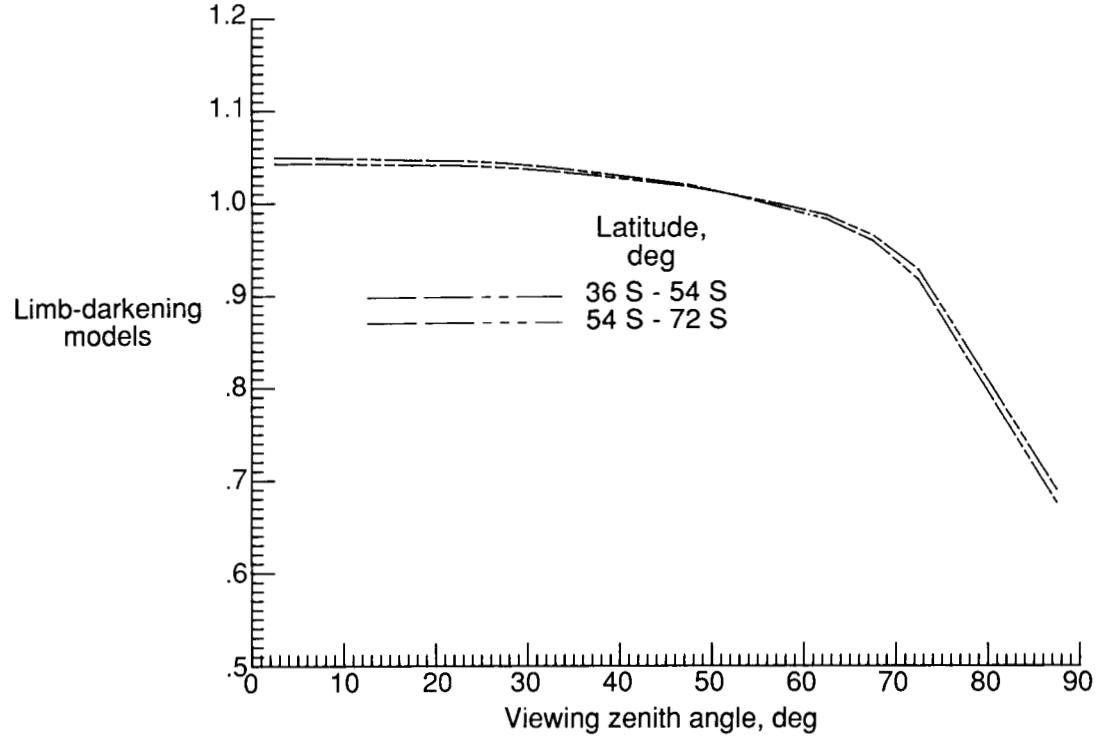

Figure 14. Limb-darkening models for overcast for day.

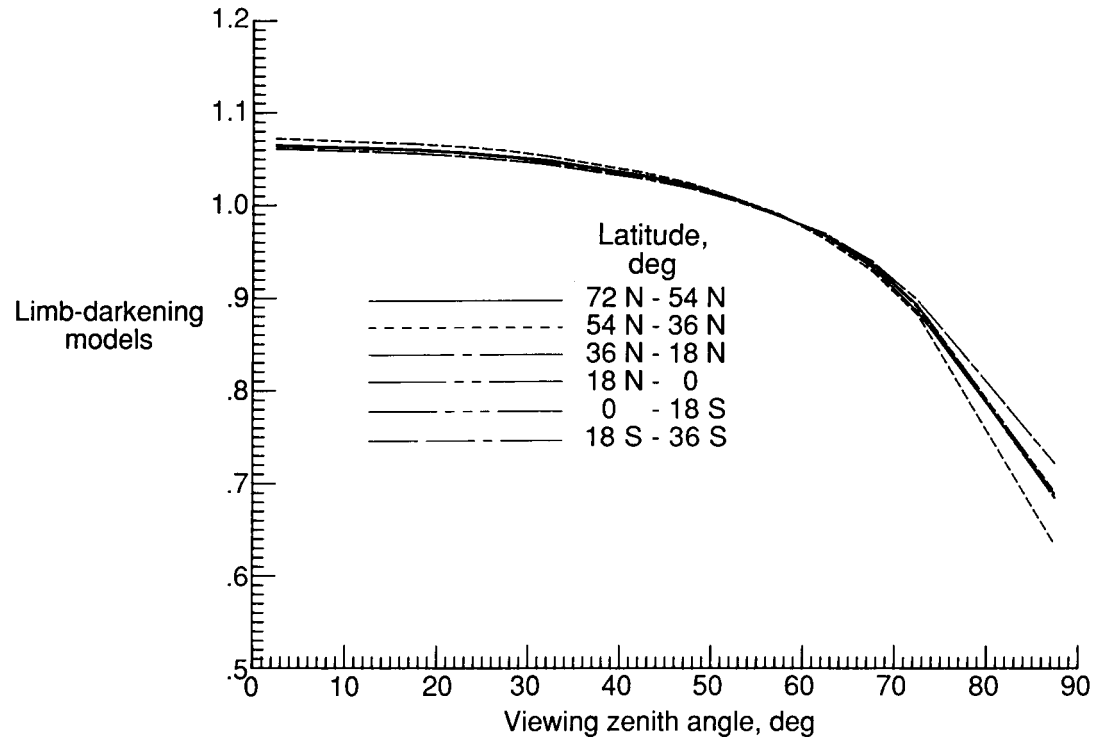

Figure 15. Limb-darkening models for clear ocean for night.

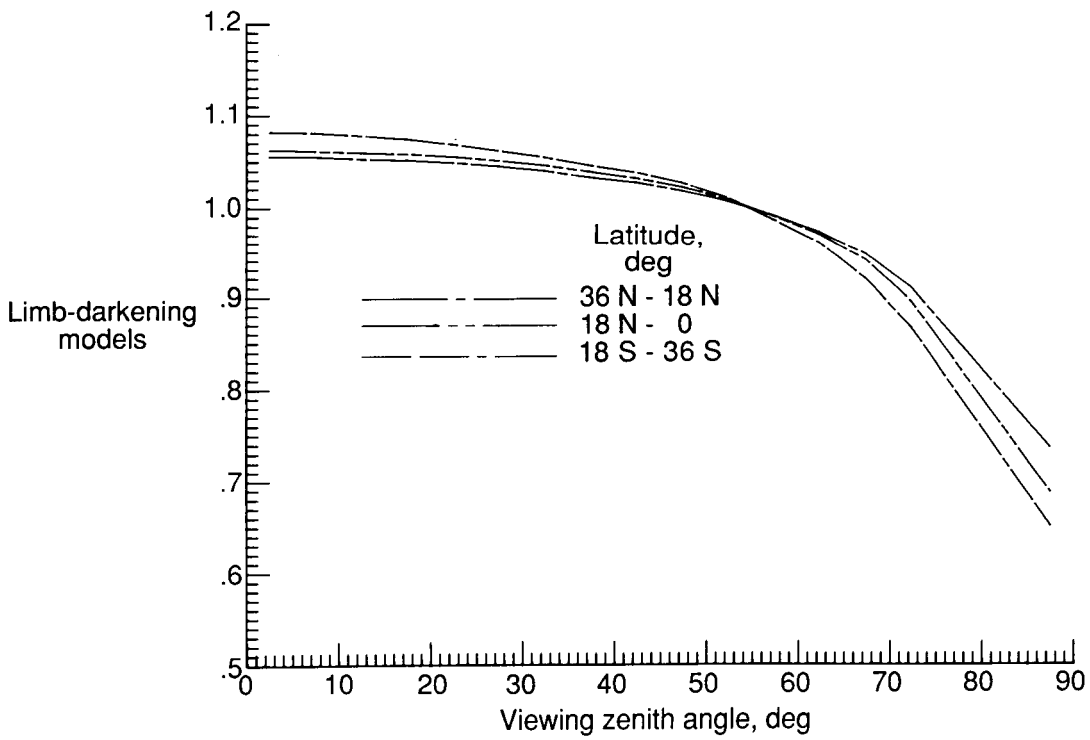

Figure 16. Limb-darkening models for clear land for night.

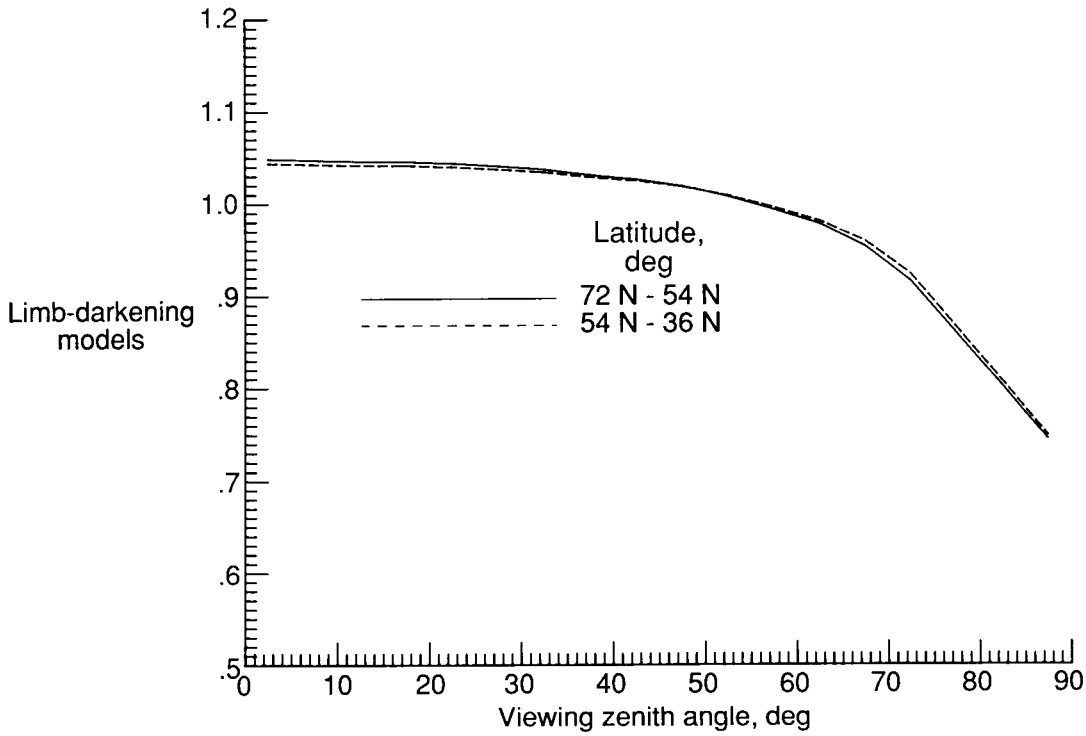

Figure 17. Limb-darkening models for clear snow for night.

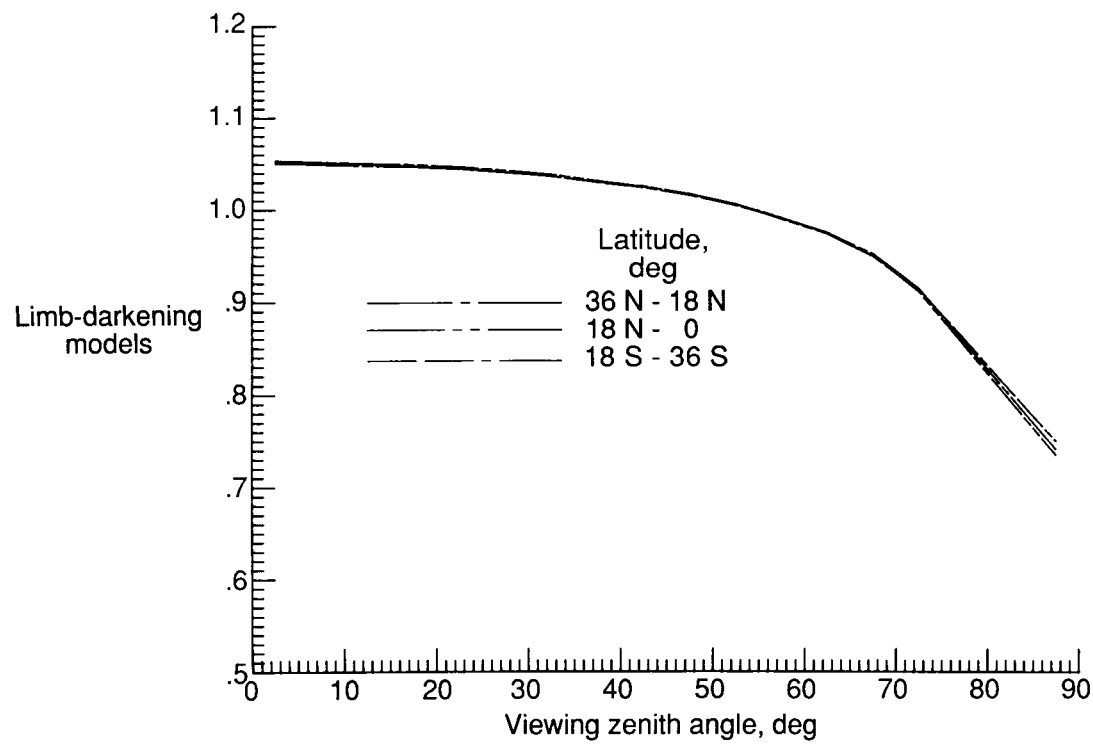

Figure 18. Limb-darkening models for clear desert for night.

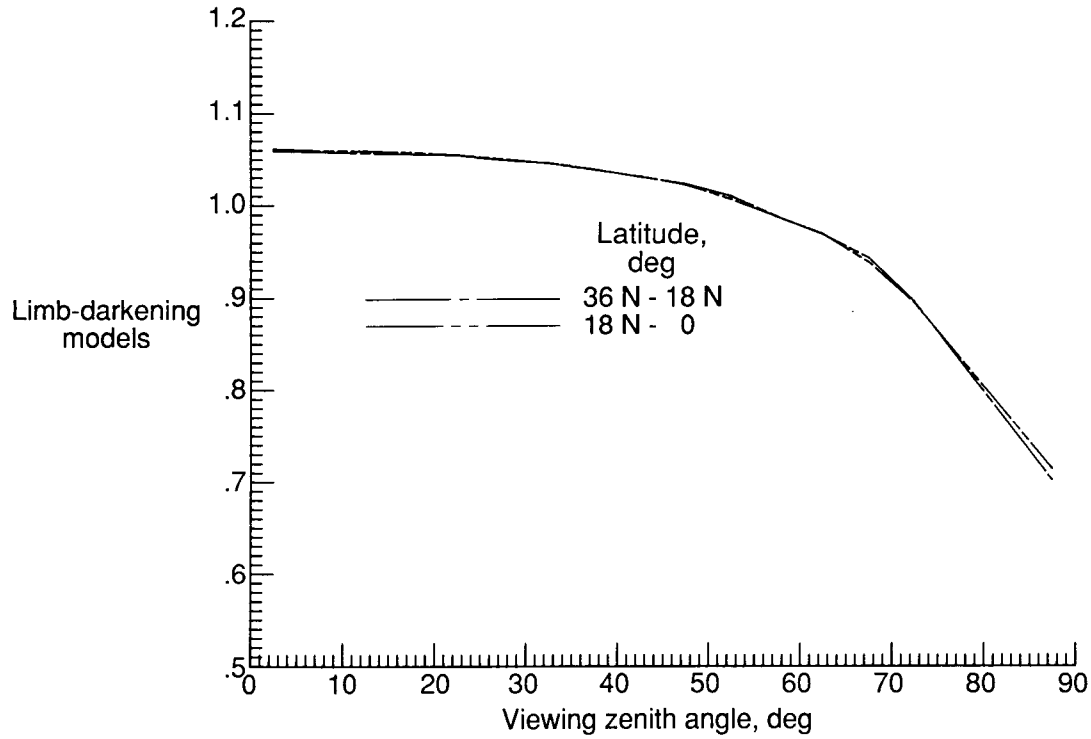

Figure 19. Limb-darkening models for clear land-ocean mix for night.

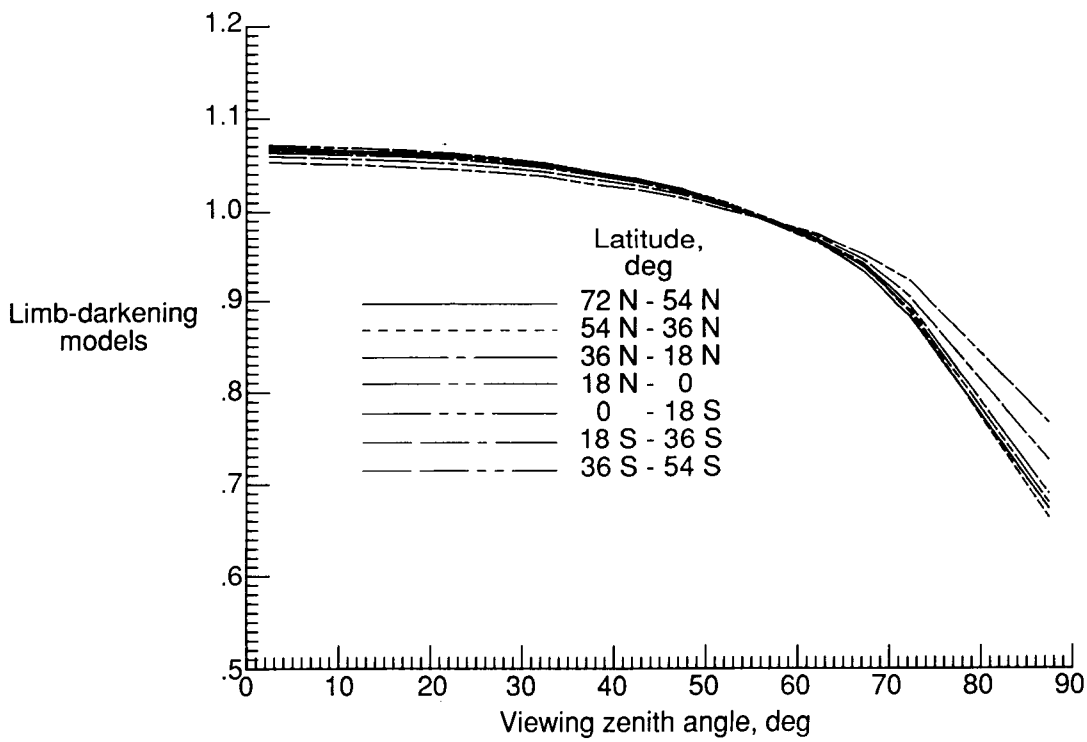

Figure 20. Limb-darkening models for partly cloudy over ocean for night.

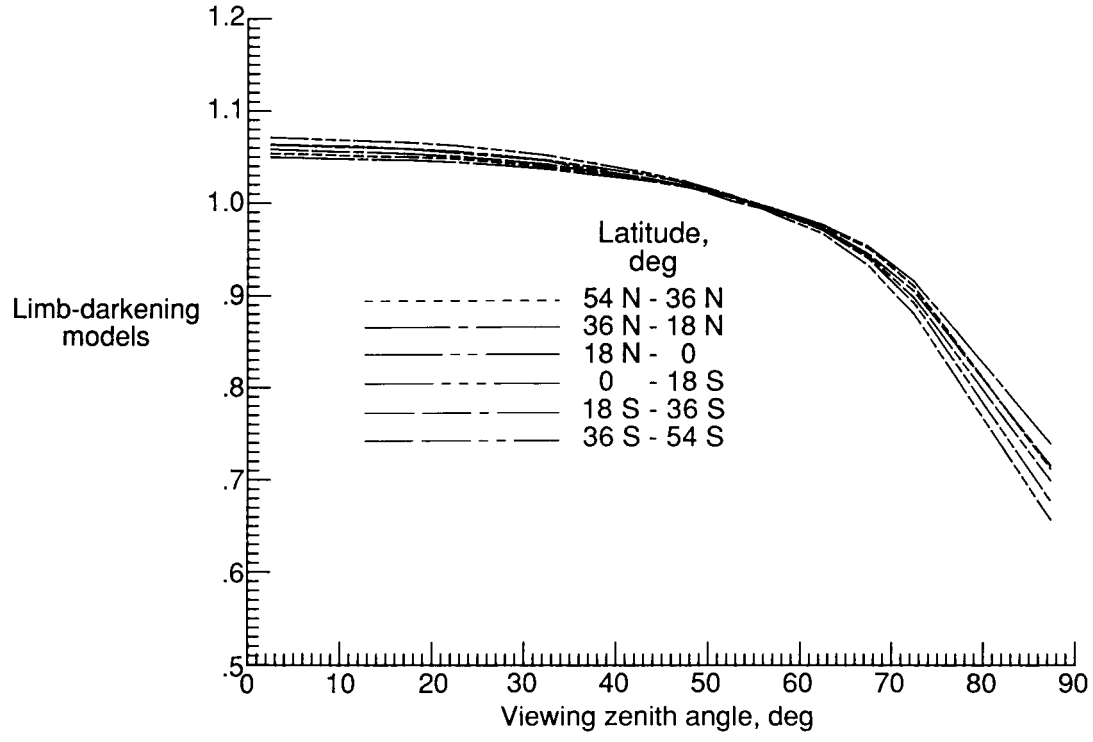

Figure 21. Limb-darkening models for partly cloudy over land for night.

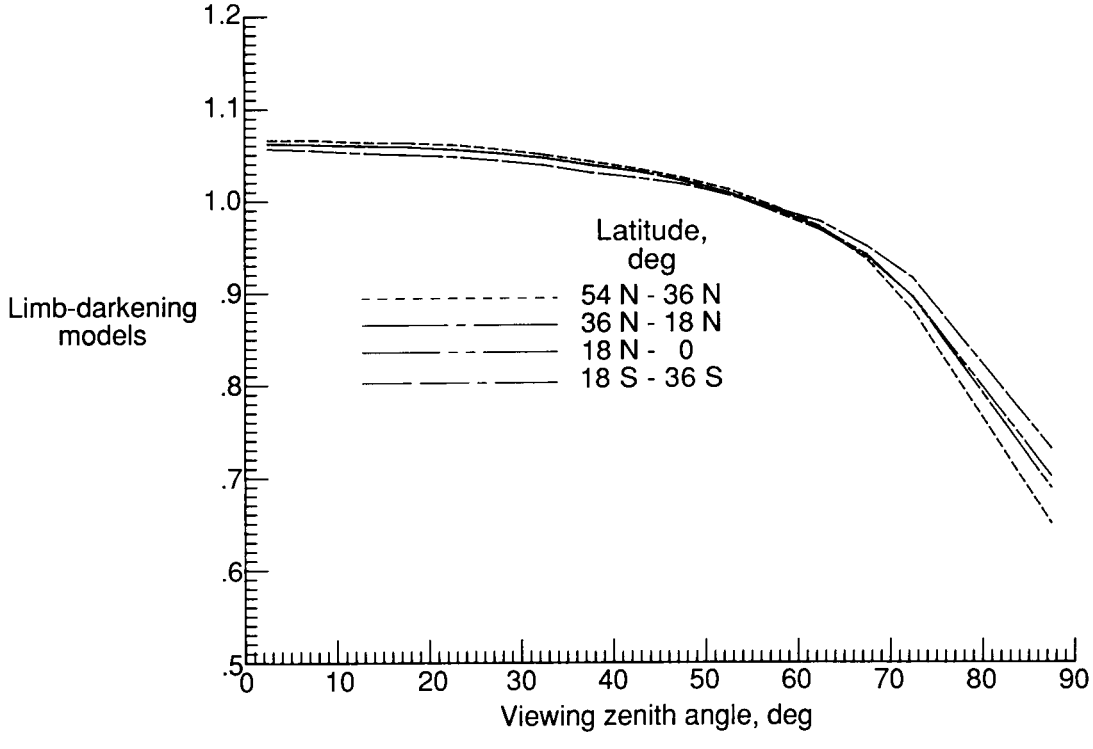

Figure 22. Limb-darkening models for partly cloudy over land-ocean mix for night.

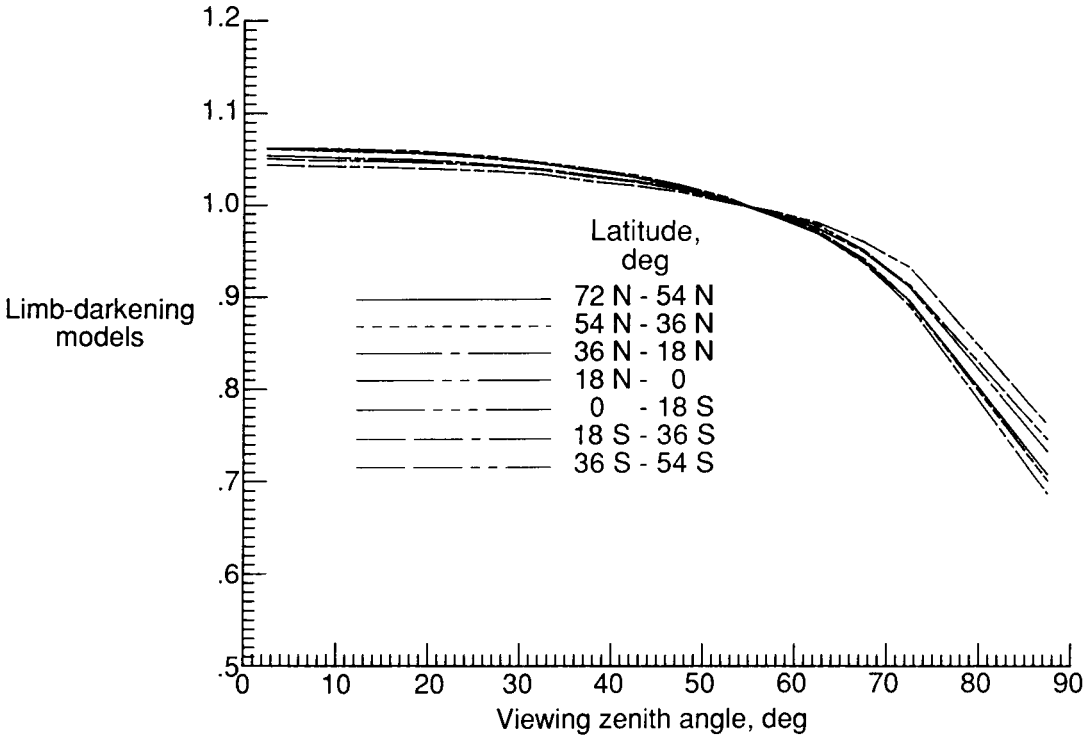

Figure 23. Limb-darkening models for mostly cloudy over ocean for night.

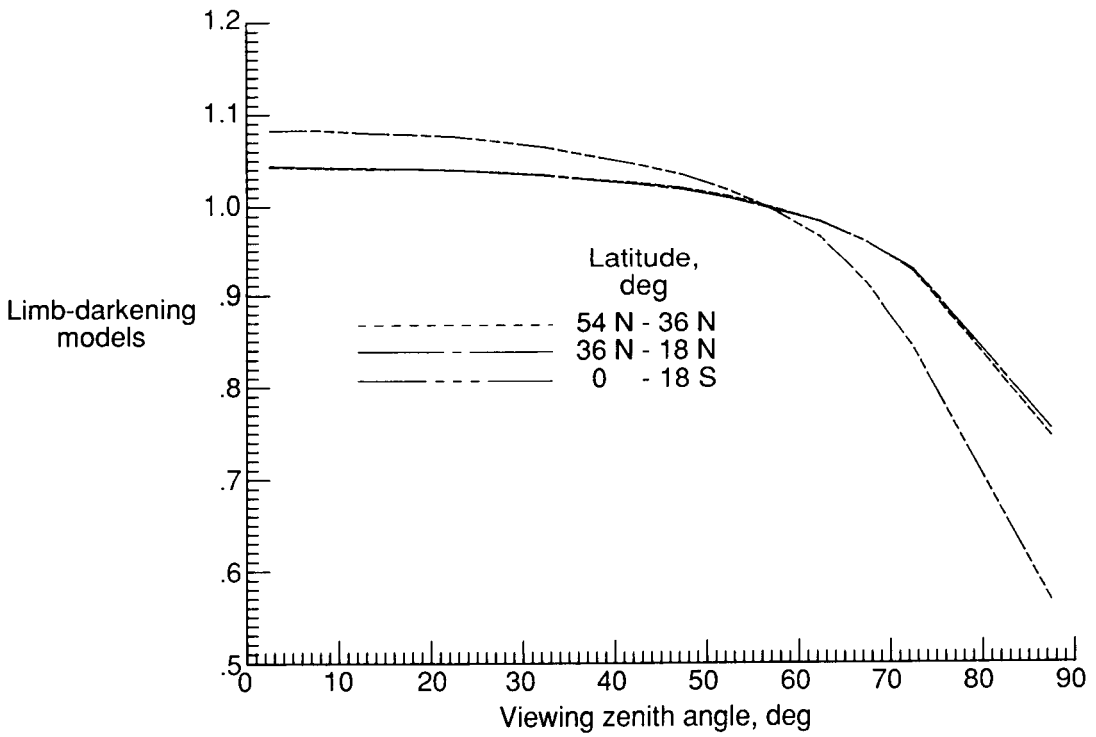

Figure 24. Limb-darkening models for mostly cloudy over land for night.

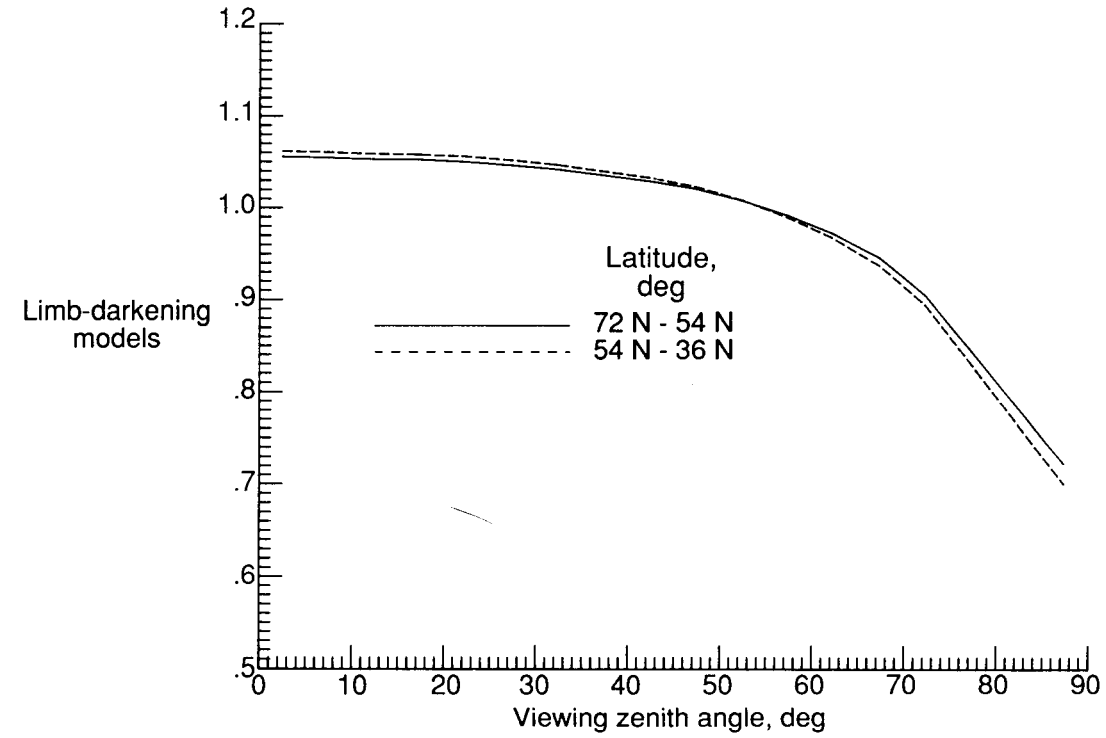

Figure 25. Limb-darkening models for mostly cloudy over land-ocean mix for night.

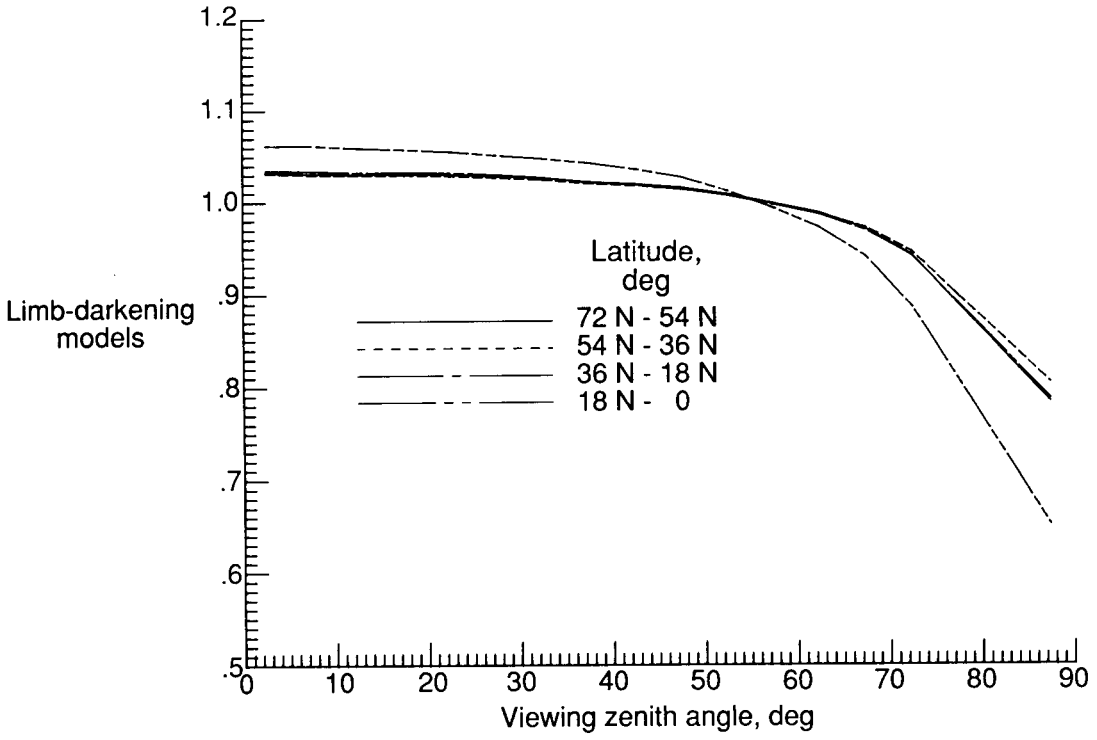

Figure 26. Limb-darkening models for overcast for night.

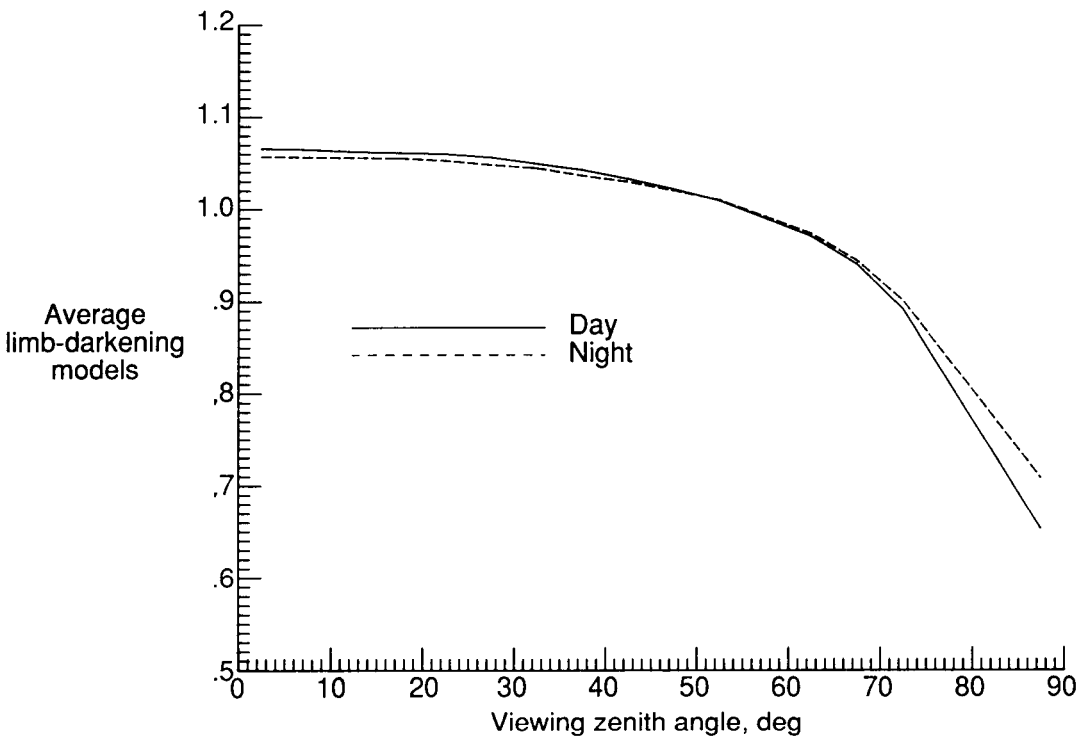

Figure 27. Average models for day and for night.

NASA
National Aeronautics and Space Administration

Report Documentation Page

1. Report No.	2. Government Accession No.	3. Recipient's Catalog No.
NASA RP-1214		

4. Title and Subtitle	5. Report Date
Limb-Darkening Functions as Derived From Along-Track Operation of the ERBE Scanning Radiometer for January 1985	March 1989
	6. Performing Organization Code
7. Author(s)	8. Performing Organization Report No.
G. Louis Smith, Natividad Manalo, John T. Suttles, and Ira J. Walker	L-16487
9. Performing Organization Name and Address	10. Work Unit No.
NASA Langley Research Center Hampton, VA 23665-5225	672-40-05-70
	11. Contract or Grant No.
12. Sponsoring Agency Name and Address	13. Type of Report and Period Covered
National Aeronautics and Space Administration Washington, DC 20546-0001	Reference Publication
	14. Sponsoring Agency Code

15. Supplementary Notes

G. Louis Smith and John T. Suttles: Langley Research Center, Hampton, Virginia.
Natividad Manalo and Ira J. Walker: PRC Kentron, Inc., Aerospace Technologies Division, Hampton, Virginia.

16. Abstract

During January 1985, the scanning radiometer aboard the Earth Radiation Budget Satellite was operated in an along-track scanning mode. These data have been analyzed to produce limb-darkening functions for Earth-emitted radiation, which relate the radiance in any given direction to the radiant exitance. Limb-darkening functions are presented in tabular form and shown as figures for 10 day cases and 12 night cases, which correspond to various scene types and latitude zones. The scene types were computed using measurements within 10° of zenith. The limb-darkening functions have values of 1.03 to 1.09 at zenith, with 1.06 being typical. It is found that latitude causes a variation on the order of 1 percent, except for zenith angles greater than 70°. These limb-darkening models are about 2 percent higher at zenith than the models derived from Nimbus 7 data.

17. Key Words (Suggested by Authors(s))	18. Distribution Statement
Limb-darkening functions Earth-emitted radiation Satellite radiation measurements Earth Radiation Budget Longwave radiation	Unclassified—Unlimited Subject Category 47

19. Security Classif. (of this report)	20. Security Classif. (of this page)	21. No. of Pages	22. Price
Unclassified	Unclassified	24	A03

NASA FORM 1626 OCT 86

NASA-Langley, 1989

For sale by the National Technical Information Service, Springfield, Virginia 22161-2171